Remote Sensing of Environment 224 (2019) 12–28

Contents lists available at ScienceDirect

Remote Sensing of Environment

journal homepage: www.elsevier.com/locate/rse

Comparison and evaluation of MODIS Multi-angle Implementation of Atmospheric Correction (MAIAC) aerosol product over South Asia

Alaa Mhawish[a], Tirthankar Banerjee[a,b,*], Meytar Sorek-Hamer[c], Alexei Lyapustin[d], David M. Broday[e], Robert Chatfield[c]

[a] Institute of Environment and Sustainable Development, Banaras Hindu University, Varanasi, India
[b] DST - Mahamana Centre of Excellence in Climate Change Research, Banaras Hindu University, Varanasi, India
[c] NASA Ames Research Center, Moffett Field, CA, USA
[d] NASA Goddard Space Flight Center, Greenbelt, MD, USA
[e] Civil and Environmental Engineering, Technion, Haifa, Israel

ARTICLE INFO

Keywords:
AERONET
AOD
MODIS
MAIAC
Aerosols
IGP
South Asia

ABSTRACT

The Multiangle Implementation of Atmospheric Correction (MAIAC) is a new generic algorithm applied to collection 6 (C6) MODIS measurements to retrieve Aerosol Optical Depth (AOD) over land at high spatial resolution (1 km). This study is the first evaluation of the MAIAC AOD from MODIS Aqua (A) and Terra (T) satellites between 2006 and 2016 over South Asia. The retrieval accuracy of MAIAC was assessed by comparing it to ground-truth AErosol RObotic NETwork (AERONET) AOD, as well as to AOD retrieved by the two operational MODIS algorithms: Dark Target (DT) and Deep Blue (DB). MAIAC AOD showed higher spatial coverage and retrieval frequency than either the DT or the DB AOD retrievals. The high spatial resolution of the MAIAC retrievals enhances the capability to distinguish aerosol sources and to determine fine aerosol features, such as wildfire smoke plumes and haze over complex geographical regions, and provides more retrievals in conditions that are cloudy or when the surface is partially covered by snow. In comparison to AERONET AOD, MAIAC AOD shows a better accuracy than both DT and DB AOD. A higher number of MAIAC-AERONET AOD matchups demonstrate the capability of MAIAC to retrieve AOD over varied surfaces, different aerosol types and loadings. Our results demonstrate high retrieval accuracy in term of the Expected Error (EE) (A/T, EE: 72.22%, 73.50%), and low root mean square error (A/T, RMSE: 0.148, 0.164), root mean bias (RMB) (A/T, RMB: 0.978, 1.049) and mean absolute error (MAE) (A/T, MAE: 0.098, 0.096). Moreover, MAIAC has a lower bias as a function of the viewing geometry and the aerosol type among the three retrieval algorithms. MAIAC performed well over bright and vegetated land surfaces, showing the highest retrieval accuracy over dense vegetation and particularly well in retrieving smoke AOD, yet it underestimated dust AOD. In conclusion, MAIAC's ability to provide AOD at high spatial resolution appears promising over South Asia, thus having advantage over contemporary aerosol retrieval algorithms for epidemiological and climatological studies.

Capsule: In comparison with MODIS DT and DB AOD, and AERONET AOD, MAIAC shows improved accuracy and lower bias over South Asia, as well as with greater spatial coverage.

1. Introduction

Aerosols are multi-component mixtures of solid and liquid particles from a wide range of natural and anthropogenic sources, and they evolve through different microphysical processes before being removed from the atmosphere by wet or dry deposition. The heterogeneity in aerosol physical, chemical, and optical properties depends on their geological and geographical nature (Ramanathan and Ramana, 2005), strength of sources (Banerjee et al., 2015; Singh et al., 2017a), and different meteorological factors (Altaratz et al., 2013). Despite their small mass and volume, aerosols have strong influence on the transfer of solar energy through the atmosphere, thereby affecting Earth's energy budget. The interaction of aerosols with solar radiation forms the primary basis of its impact on climate (i.e. direct effects) and cloud formation processes and properties (i.e the aerosol-cloud indirect effect) (Seinfeld et al., 2016). In particular, absorbing aerosols can promote cloud evaporation, leading to a reduction in cloud cover (semi-direct effect) (Hansen et al., 1997). As such, aerosols were found to

* Corresponding author at: Institute of Environment and Sustainable Development, Banaras Hindu University, Varanasi 221005, India.
E-mail address: tb.iesd@bhu.ac.in (T. Banerjee).

https://doi.org/10.1016/j.rse.2019.01.033
Received 26 February 2018; Received in revised form 18 January 2019; Accepted 28 January 2019

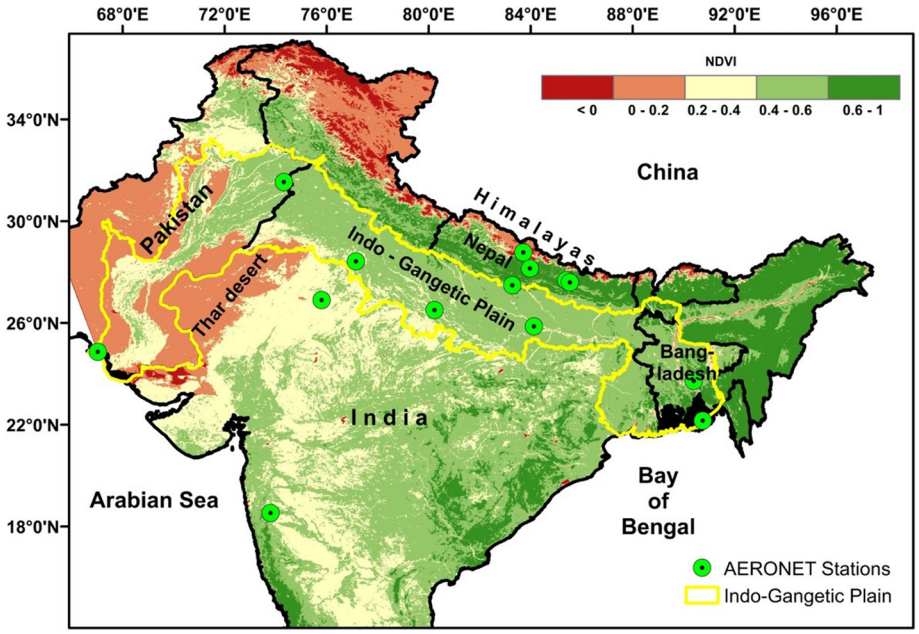

Fig. 1. South Asia study domain, with the Indo-Gangetic plain demarcated by a yellow border.
Note. The background image shows the multi-year annual average MAIAC NDVI, with dark green representing more vegetated areas and lighter shades depicting brighter surfaces. Green dots represent the location of AERONET stations used in this study. (For interpretation of the references to color in this figure legend, the reader is referred to the web version of this article.)

modify the hydrological cycle (Ramanathan et al., 2001), monsoonal pattern (Lau and Kim, 2006; Kumar et al., 2017), and thereby food security (Banerjee et al., 2018). Furthermore, aerosols are also associated with adverse health effects, including mortality and morbidity (Evans et al., 2013; Kumar et al., 2015a; Banerjee et al., 2017); they reduce visibility (Han et al., 2012), have a role in fertilization of ecosystems (Tian and An, 2013), and reduce crop yield (Burney and Ramanathan, 2014).

Following the development of various observational platforms, in particular ground-based measurements and remote sensing, as well as improved predictive models, climate-related aerosol processes are now better understood. Recent developments in Earth-observing satellites, both polar orbiting and geostationary platforms, enable us to quantify the aerosol loading and properties at a much finer spatial scale and with broader spatial and temporal coverage (Martin, 2008; Mhawish et al., 2018; Hoff and Christopher, 2009). Designated satellite sensors such as Moderate Resolution Imaging Spectroradiometer (MODIS), Multi-angle Imaging Spectroradiometer (MISR), Cloud-Aerosol LIdar with Orthogonal Polarization (CALIOP), POLarization and Directionality of the Earth's Reflectance (POLDER), Visible Infrared Imaging Radiometer Suite (VIIRS) and Ozone Monitoring Instrument (OMI) (Remer et al., 2005; Kaufman et al., 2002; Torres et al., 2007; Winker et al., 2010; Kahn and Gaitley, 2015) provide important contributions to our understanding of the effects of aerosols on climate. Among various sensors, MODIS on board the Earth Observing System (EOS) Terra and Aqua satellites are recognized as the most extensively validated sensors for retrieving aerosol properties (Remer et al., 2013; Levy et al., 2013; Bilal and Nichol, 2015; Mhawish et al., 2017). MODIS employs three independent operational aerosol retrieval algorithms: Dark Target (DT) over land (Levy et al., 2013) for dark or vegetated surfaces, DT over ocean (Tanré et al., 1997), and Deep Blue (DB), originally developed for bright surfaces (Hsu et al., 2004) but later extended to global land surface (Hsu et al., 2013). These MODIS operational algorithms are subject to continual improvement.

Lyapustin et al. (2011a, 2011b) introduced a new generic aerosol algorithm, the Multiangle Implementation of Atmospheric Correction (MAIAC), which uses MODIS L1B time series measurements and image processing and retrieves the Aerosol Optical Depths (AOD) over land at 1 km spatial resolution. Recently, MAIAC became an operational MODIS algorithm (MCD19) with Collection 6 products available from 2000 for the entire MODIS record (e.g. https://modis-land.gsfc.nasa.gov/MAIAC.html). The current version of MAIAC, used in this work, is described in Lyapustin et al. (2018). Due to the coarse spatial resolution of other standard AOD products, e.g. MODIS-DT and DB (10 km), and the low retrieval accuracy of MODIS DT 3 km (Remer et al., 2013; Mhawish et al., 2017; Gupta et al., 2018), the high 1 km resolution and the general lack of "urban" bias, MAIAC has been extensively used in the air quality and epidemiological studies (Xiao et al., 2017; Liang et al., 2018; Di et al., 2016). Intercomparison, uncertainty estimation, and validation of the retrieval algorithms are vital to build confidence in the retrieved aerosol products and to recognize the accuracy and limitations of the retrievals under different aerosol climatology and surface cover conditions. To date, MAIAC AOD has been evaluated over few geographical regions, including North America (Superczynski et al., 2017) and South America (Martins et al., 2017), and used in combination with ancillary parameters to derive surface particulate matter concentration over USA (Kloog et al., 2014; Lee et al., 2016), Mexico City (Just et al., 2015), Italy (Stafoggia et al., 2017) and Israel (Kloog et al., 2015). South Asia is a complex geo-climatic region that shows high diversity in aerosol loading and optical properties, especially over the Indo-Gangetic Plain (IGP, Sen et al., 2017; Sayer et al., 2014; Singh et al., 2017a, 2017b, 2018). Retrieval of satellite aerosol properties is therefore often challenging due to considerable seasonal variations in surface reflectance and aerosol properties (Mhawish et al., 2017, 2018). Considering these uncertainties, a first-of-its-kind effort was made to evaluate the MAIAC AOD over South Asia using AErosol RObotic NETwork (AERONET) ground-truth AOD. The retrieval accuracy of the MAIAC AOD was also compared to the two operational MODIS AOD retrieval algorithms (DT and DB). In particular, we employed a broader perspective and evaluated MAIAC performance under varying aerosol loading, aerosol types, surface coverage, and viewing geometry. Such a systematic analysis has not been reported before for South Asia, and is expected to be useful to the air quality and modeling communities, as well as for the algorithm developers.

2. Methods

2.1. Study domain

Fig. 1 shows the geographical distribution of the selected 14 AERONET sites across South Asia. These stations are located in areas that are influenced by different aerosol types (dust, smoke, urban

aerosols) and geo-climatic features (arid areas, coastal zones, elevated land, vegetation type). South Asia is one of the most densely populated regions on Earth and suffers from poor air quality particularly during post-monsoon (SON) and winter (DJF, Singh et al., 2017a, 2017b). Aerosol composition and morphology across South Asia are highly diverse, complex, and dynamic, due to prevalence of different sources and varying meteorological conditions. Recently, Singh et al. (2017a) reviewed sources of fine particulate matter ($PM_{2.5}$) across South Asia and found considerable spatial and seasonal source variation, with an overall dominance of vehicular emissions, industrial emissions, secondary aerosols, and biogenic sources. The region is highly affected by pre-monsoon (MAM) mineral dust, transported from the north-western deserts (e.g. the Thar desert) and from the dry western regions of Pakistan, Afghanistan and the Arabian Peninsula (Gautam et al., 2010). In contrast, during post-monsoon and winter the entire northern part is affected by smog (smoke and fog) and by emissions from burning of agricultural crop residues and waste material (Sen et al., 2017; Singh et al., 2018).

2.2. Data

MODIS sensors on board Terra and Aqua satellites provide columnar aerosol properties since 2000 and 2002, respectively. Being part of the A-Train constellation, Aqua MODIS crosses the equator on 13:30 local time while Terra crosses the equator on 10:30 local time. The MODIS sensor has 36 spectral bands with different spatial resolutions (250, 500 and 1000 m), and a 2330 km wide swath, providing near-daily global coverage by each single instrument (T/A). The MODIS aerosol retrieval algorithms have been updated several times and three operational algorithms (DT, DB and MAIAC) are currently in use to retrieve AOD. In the present analysis, we used collection 6 (C6) data products for all MODIS aerosol algorithms.

2.2.1. MAIAC AOD

MAIAC processing algorithm is based on a dynamic time series analysis that allows separating surface properties which are relatively static during short time intervals from features that rapidly change over time, like aerosols and clouds (Lyapustin et al., 2018). MAIAC starts with gridding the MODIS Top-Of-Atmosphere (TOA) L1B reflectance to 1 km resolution on a fixed grid. The gridded data are split into 1200 km tiles and placed in a queue containing from 5 (over the poles) to 16 (over the equator) days. This provides a (backward) time dimension for each 1 km grid cell. MAIAC cloud mask is combined with the detection of absorbing aerosols (smoke or dust) allowing MAIAC to characterize most of the aerosol emission sources at 1 km resolution, including high intensity plumes, without masking them as clouds.

Central to the MAIAC aerosol retrieval is characterization of the surface reflectance spectral ratios (SRC) 0.47/2.13 and 0.47/0.55 using the minimum reflectance method (Lyapustin et al., 2018). The code uses MAIAC cloud mask but otherwise is run independently from the main MAIAC processing, providing separation between the surface and atmospheric contributions to the TOA signal. Importantly, this code runs dynamically and updates the SRC on a continuous basis. The angular dependence of the SRC is accounted for by using three angular bins.

The AOD retrieval algorithm uses different band combinations, including 0.47, 0.55, 0.65 and 2.13 μm, depending on the surface brightness and the detected aerosol type (for details, see Lyapustin et al., 2018). Aerosol information, along with the retrieved column water vapor (CWV) from MODIS NIR measurements at 0.94 μm (Lyapustin et al., 2014), are used for atmospheric correction and spectral bidirectional reflectance distribution function (BRDF) retrieval. Once the surface BRDF is derived, it is synergistically used for cloud/cloud shadow/snow detection, determination of the aerosol type, and in aerosol retrieval. Finally, spatio-statistical filtering of high AOD values at 1 km allows for residual cloud detection and for overall improvement of the aerosol and surface products.

MAIAC uses geographically prescribed aerosol models based on the aerosol climatology obtained from AERONET. The current MAIAC aerosol models are static and do not account for seasonal variations of the aerosol properties, which is one of the limitations of the MAIAC C6 aerosol product. In the current study, AODs with the highest quality at 0.55 μm have been used. We also used MAIAC 8-day composite NDVI product at 1 km resolution as a proxy of the surface cover types.

2.2.2. Dark target AOD

The MODIS DT algorithm was developed to retrieve aerosols over dark vegetated land surfaces at 10 km spatial resolution, using statistical relationship between the visible bands at 0.47 and 0.65 μm and the shortwave infrared band at 2.12 μm to determine the surface reflectance (Levy et al., 2013). For AOD retrieval, the DT algorithm selects suitable dark pixels (500 m resolution) with 0.01 to 0.25 TOA reflectance in the 2.12 μm channel. The selected pixels are organized into 20 × 20 (400 pixel) array and after screening out cloud, water, snow/ice and other bright pixels, the algorithm discards the darkest 20% and the brightest 50% (in the 0.65 μm channel) pixels. The reflectance of the remaining pixels is averaged and used to derive the AOD, and the retrieval quality is determined by the number of pixels used. The DT algorithm over land uses three fine aerosol models (low-, moderate- and highly absorbing) and one coarse aerosol model, with the prescribed model selection depending on the season and geographical location. The C6 DT product provides AOD retrievals at two spatial resolutions: 10 km and 3 km, using similar yet not identical retrieval algorithms. Namely, the difference between the 3 km and 10 km AOD is in the selection of pixels for which the retrieval is performed. In this study, we used the DT 10 km AOD product rather than the more spatially resolved DT 3 km AOD due to the higher retrieval accuracy of the former, especially over urban areas (Gupta et al., 2018; Mhawish et al., 2017; Nichol and Bilal, 2016; Munchak et al., 2013). The reported expected error (EE) of DT AOD over land is ± (0.05 + AOD15%) (Levy et al., 2013).

2.2.3. Deep blue AOD

The MODIS DB algorithm was originally developed to retrieve AOD over bright surfaces, including deserts, at 10 km spatial resolution, utilizing the 0.412 and/or 0.47/0.65 μm wavelengths depending on the surface type (Hsu et al., 2013; Sayer et al., 2015; Tao et al., 2017). The C6 (enhanced) DB algorithm extends retrievals to green and dark surfaces and provide global AOD except over snow and ice. Over vegetated surfaces, the DB algorithm uses statistical spectral ratios as a function of NDVI for determining the surface reflectance, similar to the DT algorithm. Over bright surfaces, it relies on static seasonal database of spectral surface reflectance, binned in view geometry, and derived from the previous years of MODIS measurements, based on the minimum reflectance method. The DB algorithm selects the aerosol model as a function of the geographical location and the season. The AOD and the Angstrom Exponent (AE) are retrieved for fine and mixed aerosol conditions, while AOD and the single scattering albedo (SSA) are retrieved when dust is detected. The DB algorithm retrieves AOD at a 1 km nominal resolution and filters data for bad quality or residual clouds before aggregating it to 10 km, unlike the DT algorithm which aggregates the radiance first to 10 km using the darkest eligible pixels and only then performs aerosol retrieval.

2.2.4. AERONET

AERONET is a worldwide ground-based sun photometer network that provides aerosol optical properties with high temporal resolution (AOD: 5–15 min, sky radiance: 30 min). AERONET provides cloud screened AOD at several wavelengths between 340 and 1640 nm with ~ ± 0.01 accuracy at wavelengths > 440 nm and ~ ± 0.02 at shorter wavelengths (Holben et al., 1998). AERONET Version 2 Level 2.0 quality-controlled AOD data were compared to MODIS AOD. For this,

AERONET AOD (AOD_{AER}) at 500 nm was interpolated to 550 nm using AE of the 440 nm and 675 nm wavelength pair. The MODIS AOD at 550 nm was obtained using the three retrieval algorithms: MAIAC, DT and DB. Other AERONET aerosol products, such as the AE based on the 440 nm and the 870 nm wavelengths, the SSA at four wavelengths (440, 675, 870 and 1020 nm), and the CWV were used to determine the dominant aerosol type (Dubovik and King, 2000) and size fraction (O'Neill et al., 2001). Based on data availability (at least 1 year), 14 AERONET stations across South Asia were used (Table S1).

2.3. Data processing

AERONET provides point AOD measurements with high temporal resolution whereas MODIS provides spatial AOD measurements during the satellite overpass time, at most once per day. Thus, in order to match the AERONET AOD with the MODIS AOD, we averaged (a) the AERONET AOD over a temporal window of ± 60 min around the satellite overpass time and (b) the MODIS AOD over a spatial window of 3 × 3 pixels centered at each of the AERONET sites. Only the highest quality AOD data (MAIAC: highest quality, DT: QA = 3, DB: QA ≥ 2) have been used, to avoid cloud contamination and other errors in the AOD retrieval. To avoid artifacts, the MODIS-AERONET AOD matchups were retained only when at least two retrieved pixels were recorded within the 3 × 3 spatial window for each aerosol product and the AERONET temporal window (T: 9.30–11.30, A: 12.30–14.30 local time). The 3 × 3 pixel window translates into a 3 × 3 km^2 averaging area for MAIAC, regardless of the view angle, and a 30 × 30 km^2 area (at nadir) for DT and DB.

Table 1 reports the MODIS and AERONET aerosol products used in this study. Terra and Aqua MODIS geometry parameters (scattering angle, viewing zenith angle, and relative azimuth angle) were used for studying the angular dependence of the AOD retrieval bias. The 8-day composite NDVI was used for examining the impact of surface cover on AOD retrieval bias. For spatial comparison of MAIAC-, DT- and DB AOD over South Asia, a multiyear AOD average and the retrieval frequency were computed. To unify the spatial resolution of all the MODIS products, the MAIAC AOD at 1 km were resampled to 10 km, using the nearest neighbor method. Aggregating MAIAC AOD to 10 km resolution does not affect the accuracy of the data, since the nearest neighbor resampling technique averages all the pixels within a 10 km grid.

Several statistics were used to assess the retrieval accuracy of the different MODIS algorithms, including the root mean square error (RMSE), mean absolute error (MAE), relative mean bias (RMB), and the expected error (EE), with the later defining the radial boundaries in which 67% of the matched AERONET and MODIS points fall. We used the EE definition of the dark target algorithm ± (0.05 + 0.15 AOD_{AER}).

3. Results and discussion

3.1. Spatial intercomparison of MAIAC, DT and DB

Considering the heterogeneity of aerosol sources, types, and loading that persists over South Asia and especially over the IGP, the spatial intercomparison between MAIAC-, DT- and DB AOD was made. The performance of the three MODIS aerosol retrieval algorithms were examined for selected events (e.g. haze, smoke, and dust), using visual analysis of MODIS true color images. Next, using multi-year averaging of the annual and seasonal AOD, we investigated the spatial and temporal variation of AOD retrieval, the retrieval frequency, and the spatial coverage of the retrieval algorithms.

3.1.1. Special events

Fig. 2 shows true-color images of haze, dust, and a smoke plume, as well as the MAIAC-, DT- and DB AOD retrieval for these aerosol types. The IGP are frequently affected by serious haze-fog conditions during the winter (Mhawish et al., 2017; Kumar et al., 2015b) whereas dust storms over southwest IGP and north-northwestern India are common during pre-monsoon (Gautam et al., 2010). Aqua MODIS true-color image (Fig. 2a) shows thick smoke layer extending along the IGP region on the 21 December 2016. Both MAIAC and DB succeeded to retrieve the thick smoke AOD while DT retrievals failed under clear-sky conditions. The failure of DT to retrieve heavy smoke AOD could be attributed to the bright surface mask or the cloud mask. The DT algorithm also failed to retrieve heavy dust (Fig. 2b) over both bright and dark surfaces, in contrast with MAIAC and DB that successfully retrieved the AOD during dust events. The presence of large dust particles in the atmosphere reduces the TOA reflectance at 2.13 μm. Since the DT algorithm assumes that the atmosphere is transparent at 2.13 μm, the VIS-SWIR surface reflectance relationship under such conditions is poor. Owing to its fine spatial resolution, the retrieved MAIAC AOD shows richer spatial patterns and superior fine features, such as wildfire smoke plume (Fig. 2c) and haze over a complex geographical region and between clouds/snow in the Kashmir valley, India (Fig. 2d). This demonstrates the advantage of using the MAIAC high-resolution aerosol data for epidemiological/climatological studies.

3.1.2. Spatial and temporal variation of MODIS AOD retrievals

Significant spatial and temporal variations in aerosol loading (Fig. 3) and the retrieval frequency (Fig. 4) are observed across South Asia. The MAIAC and DB AOD spatial coverage are higher compared to DT AOD due to their ability to retrieve AOD over both dark and bright surfaces. Additionally, the high spatial resolution of MAIAC enables retrievals of AOD over complex landscapes, such as the Baluchistan region, the Himalayan foot-hills, the coastal line, and in between clouds. In contrast, the DT and DB algorithms cannot retrieve fine aerosol feature due to their inherently coarser spatial resolution (10 km). All the algorithms showed a similar AOD spatial pattern, with higher values over IGP (thick line boundary; area weighted mean ±

Table 1
Summary of data used for the MODIS-AERONET comparative analysis.

Instrument/products	SDS name	Description	Resolution
AERONET	Aerosol Optical Depth (V2) & AE (α)	Version 2 Direct Sun, Level 2	
	Water (cm)		
	SSA_440,675,870,1020	Version 2 Inversion, Level 2	
MOD04_L2 (Terra)	Optical_Depth_Land_and_Ocean	DT AOD at 550 nm over land and ocean	10 km
MYD04_L2 (Aqua)	Deep_Blue_Aerosol_Optical_Depth_550_Land_Best_Estimate	DB AOD at 550 nm over land	
MAIACAAOT (Aqua)	Optical_Depth_550	Aerosol Optical Depth at 550 nm	1 km
MAIACTAOT (Terra)	AOT_QA	Quality Assurance	1 km
	Scattering_Angle	Scattering Angle	5 km
	RelAZ	Relative azimuth angle	5 km
	VZA	View Zenith Angle	5 km
MAIACVI	NDVI	8-day composite NDVI	1 km

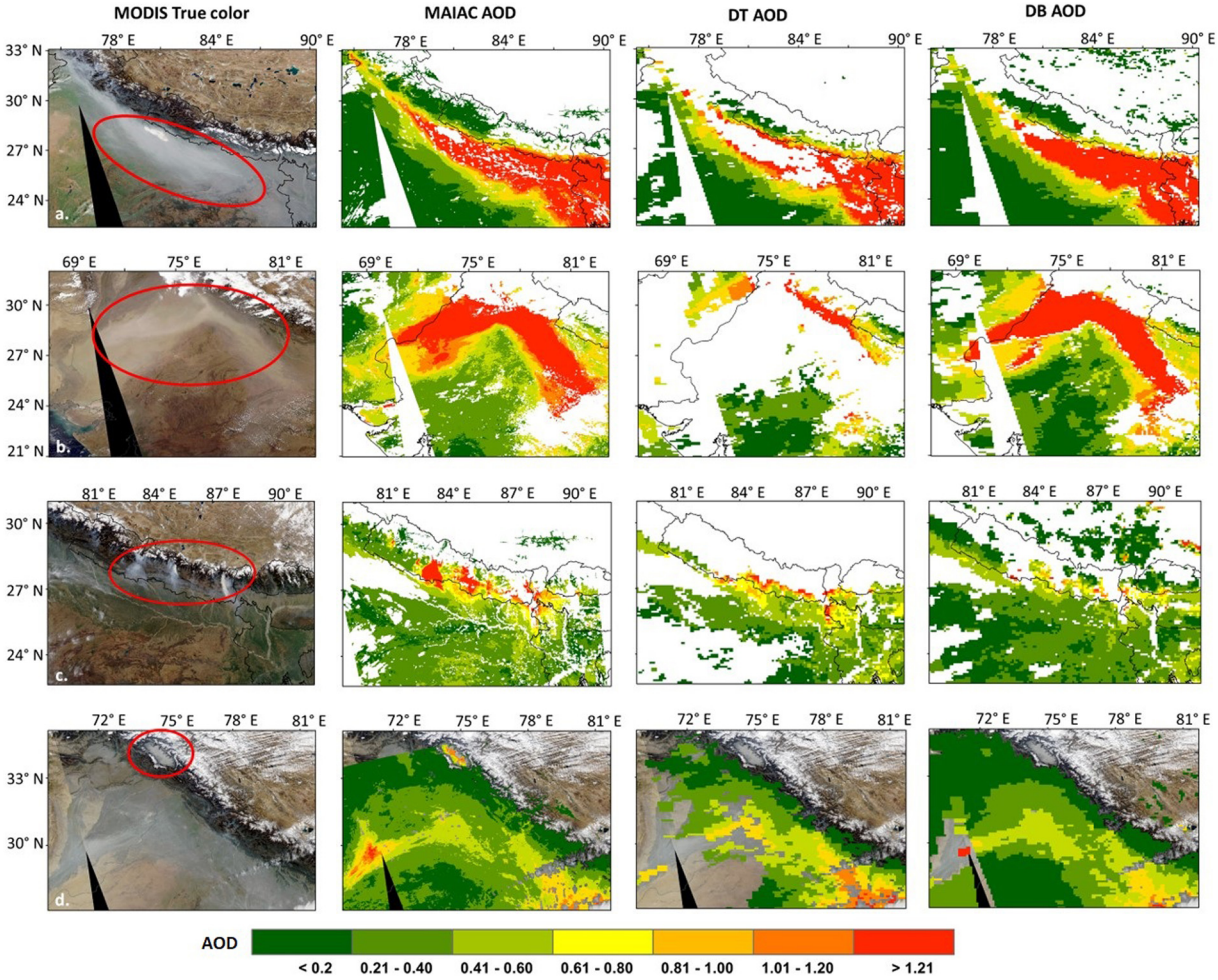

Fig. 2. A comparison between MAIAC-, DT- and DB AOD retrievals for specific events (red enclosure): (a) smoke, 21 December 2016, (b) dust, 21 April 2010, (c) forest fire, 12 March 2009, and (d) smog and in between cloud/snow cover, 5 December 2014. (For interpretation of the references to color in this figure legend, the reader is referred to the web version of this article.)

SD, MAIAC: 0.60 ± 0.10, DT: 0.63 ± 0.12, DB: 0.50 ± 0.12) compared to overall South Asia (MAIAC: 0.44 ± 0.18, DT: 0.40 ± 0.17, DB: 0.33 ± 0.16). The differences among the three algorithms are likely due to surface reflectance assumptions and/or assumptions related to the aerosol properties. The regional coverage and range of the AOD for the three algorithms differ considerably in both their spatial and temporal scale (Table S2). During dominance of pre-monsoon coarser aerosol, the spatial disagreement between the algorithms was higher, with higher MAIAC (IGP: 0.51 ± 0.10, South Asia: 0.33 ± 0.13) and DT AOD retrievals (IGP: 0.52 ± 0.10, South Asia: 0.38 ± 0.13) almost everywhere compared to DB AOD (IGP: 0.41 ± 0.08; South Asia: 0.33 ± 0.13). The highest AOD was always retrieved during monsoon (JJA) (South Asia; MAIAC: 0.57 ± 0.25, DT: 0.54 ± 0.25, DB: 0.38 ± 0.26), attributed mainly to hygroscopic growth of aerosol particles (Altaratz et al., 2013). A significant variation in the mean AOD was evident over IGP during monsoon among the three algorithms (MAIAC: 0.77 ± 0.16, DT: 0.86 ± 0.19, DB: 0.62 ± 0.21), indicating uncertainties in the aerosol optical properties assumptions. During post-monsoon, the spatial coverage of each retrieval algorithm (especially of DT) improved due to the increase in the surface vegetation cover (Fig. S1). During winter, aerosol climatology is mainly associated with intense biomass and agricultural waste burning, especially over the upper IGP, with similar DT AOD (IGP: 0.59 ± 0.15, South Asia: 0.36 ± 0.19), DB AOD (IGP: 0.49 ± 0.19, South Asia: 0.33 ± 0.18), and MAIAC AOD (IGP: 0.55 ± 0.17, South Asia: 0.37 ± 0.20).

The retrieval frequencies among the three algorithms varied considerably, mainly attributed to the cloud cover, surface type, and the ability of each algorithm to retrieve different aerosol types (e.g. smoke and dust, Fig. 4). Retrieval frequency was higher over the southwest Indian peninsula (> 220 days/year), mainly due to minimal cloud coverage compared to Nepal and the east and south Indian peninsula (Cai et al., 2017). During monsoon, the high cloudiness conditions reduce the retrieval frequency of all the algorithms significantly, with a comparatively higher retrieval frequency over Pakistan due to lower cloud coverage. In general, MAIAC performed slightly better than DB in terms of retrieval frequency, which is attributed to the higher spatial resolution of MAIAC. MAIAC also enabled retrieval over complex geographical regions and between clouds/snow. The DT retrieval frequency is low over the upper IGP, which is dominated by sparse and non-vegetated surfaces (Fig. S1). The retrieval frequency increases during post-monsoon, especially over Pakistan and north-west India, with MAIAC again outperforming the DB and DT. In winter, the retrieval frequency remains relatively uniform (46–75 days) with maximum retrieval over the central Indian subcontinent (south Pakistan and central India). Overall, MAIAC showed a higher number of retrievals than DT and DB in all seasons, demonstrating its capability to retrieve AOD under different surface and aerosols type conditions. In terms of spatial coverage, the performance of DB was very close to that of MAIAC whereas DT showed inferior spatial coverage at low AOD conditions over bright and sparsely vegetated land (Mhawish et al., 2017).

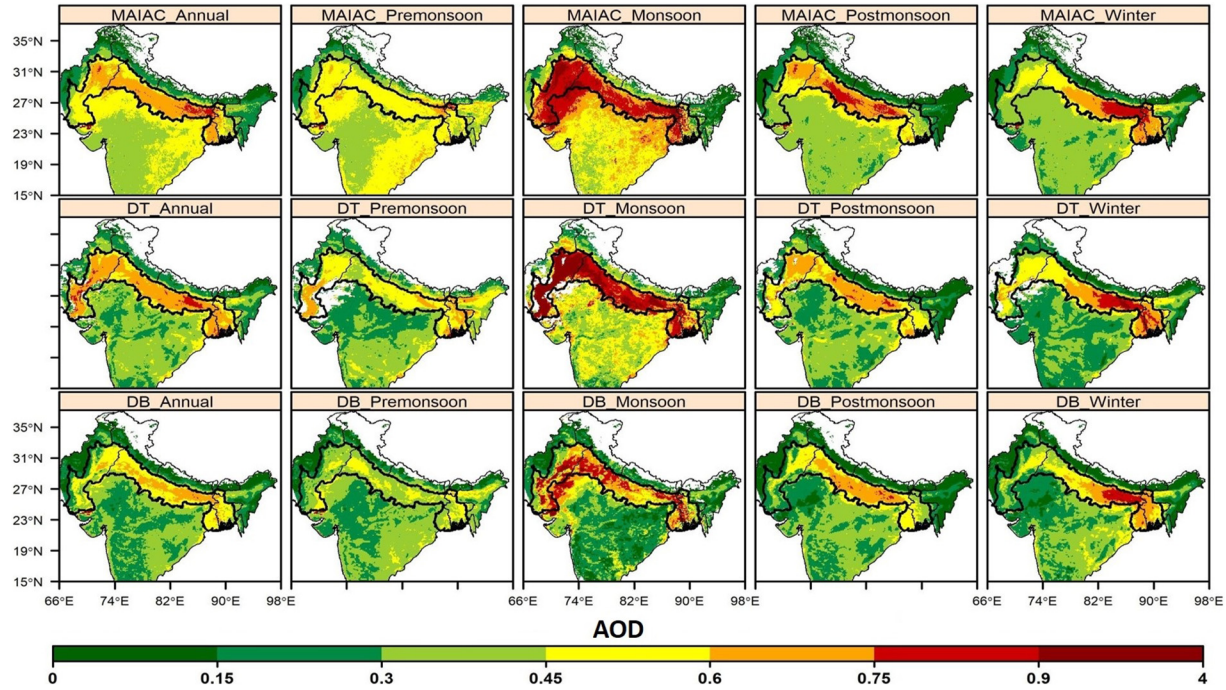

Fig. 3. Spatial distribution of annual and seasonal means of MAIAC-, DT- and DB AOD, retrieved over South Asia from 2006 to 2016. The area demarcated with bold border represents the IGP region.

To compare the spatial and temporal variation of AOD retrievals by the different algorithms the geographical distribution of the annual and seasonal mean differences between MAIAC and DT AOD and between MAIAC and DB AOD were plotted in Fig. 5. The mean difference between MAIAC and DB AOD was found to be positive over almost the entire South Asia, with the highest discrepancies (> 0.35) observed over arid areas (the Thar desert between India and Pakistan, Baluchistan in central west Pakistan), where coarse aerosols are common. This suggests that low DB AOD are retrieved due to the overestimation of the surface reflectance and/or due to inaccurate assumptions of the coarse aerosol model. The spatial variation of the differences between MAIAC and DT AOD showed two patterns: 1) negative annual mean differences over the northern Indian subcontinent, ranging from -0.05 (middle IGP) to -0.35 (Indus valley plain of Pakistan, and Bangladesh), and 2) positive annual mean differences over the rest of South Asia, ranging from 0.05 to 0.35, and negligible differences (-0.05 to 0.05) over the central part of IGP. Temporally, the MAIAC AOD differences against DT and DB AOD varied, with the highest differences of both DT and DB from MAIAC found during monsoon. The consistency between the three algorithms was better during winter and postmonsoon, when the aerosols are dominated by fine mode particles. Furthermore, DT showed higher consistency with MAIAC in all the seasons over South Asia and IGP compared to DB, with the latter showing a significant underestimation of AOD.

3.2. Evaluation of MAIAC, DT and DB AOD against AERONET AOD

3.2.1. Evaluation of MAIAC, DT and DB AOD

The retrieval accuracy of MAIAC AOD against DT and DB AOD over land was considered in terms of the retrievals falling within the estimated uncertainty from the average ($\pm 1\sigma$), RMSE, RMB and MAE (Fig. 6). MODIS AOD from both the Terra (T) and Aqua (A) satellites was examined for consistency. The 3×3 pixel retrieval box (averaging window) translates into a $3 \times 3\,km^2$ area for MAIAC, regardless of the view angle, and a $30 \times 30\,km^2$ area for DB and DT at nadir (and grows significantly toward the edge of the scan). Fig. 6 compares Aqua and Terra MAIAC, DT and DB AOD against AOD retrievals from 14 AERONET stations, with descriptive statistics presented in Table 2. Within each algorithm, the differences between the A/T MODIS AOD were $< 2\%$ (EE), 0.015 (RMSE), and 0.01 (R). In contrast, the (A/T) AOD differences among the retrieval algorithms from a given MODIS instrument varied considerably.

For all the scenarios, MAIAC AOD outperformed the DT and DB AOD in terms of the fraction of the retrievals that fall within the EE, and exceeded the satisfactory level of the total matchups falling within the EE, with 72.22% (A, N: 6432) and 73.50% (T, N: 7227). Moreover, MAIAC showed significantly lower RMSE (A, T: 0.148, 0.146) and MAE (A, T: 0.098, 0.096) compared to the DT and DB (RMSE > 0.183, MAE > 0.122), with no significant difference between the sensors (A/T). Interestingly, both the DT and DB algorithms did not achieve satisfactory levels of retrieval (EE: 49.38–64.98%). In general, DT overestimated the AOD (RMB > 1), especially in monsoon, while DB underestimated the AOD (RMB < 0.8), with $> 40\%$ of the records falling below the EE. The significant underestimation of DB 10 km AOD indicates a considerable overestimation of the surface reflectance and/or of the aerosol SSA, whereas the overestimation by DT is due to underestimation of the surface reflectance (Mhawish et al., 2017). Unlike DT, which can only retrieve AOD over surfaces for which the modeled reflectance is $0.01 < \rho_{2.13} < 0.25$, both MAIAC and DB can retrieve AOD over any land surfaces (except snow/ice). Hence, the number of matchups for MAIAC (A: 6432, T: 7227) and DB (A: 6027, T: 6989) is significantly higher than for DT (A: 5229, T: 5984), with the higher MAIAC resolution enabling more matchup points, especially over complex land surfaces, coastlines, and in between snow and clouds (Lyapustin et al., 2011a, 2011b). For instance, while both DB and DT failed to retrieve AOD over the Jomsom AERONET station, which is located at the Himalayan foothills and dominated by low aerosol loading (mean AERONET AOD: 0.053), MAIAC was able to retrieve AOD with 71.33% (T) and 78.57% (A) of the retrievals falling within the EE (Table S3). Furthermore, among the 14 AERONET stations, MAIAC achieved better retrieval accuracy (within EE) in the majority of the stations (A: 11, T: 12), far greater than DT (A: 7, T: 9) and DB (A: 2, T: 5). The only station for which MAIAC did not achieve satisfactory retrieval was Dhaka, where it significantly underestimated the AOD.

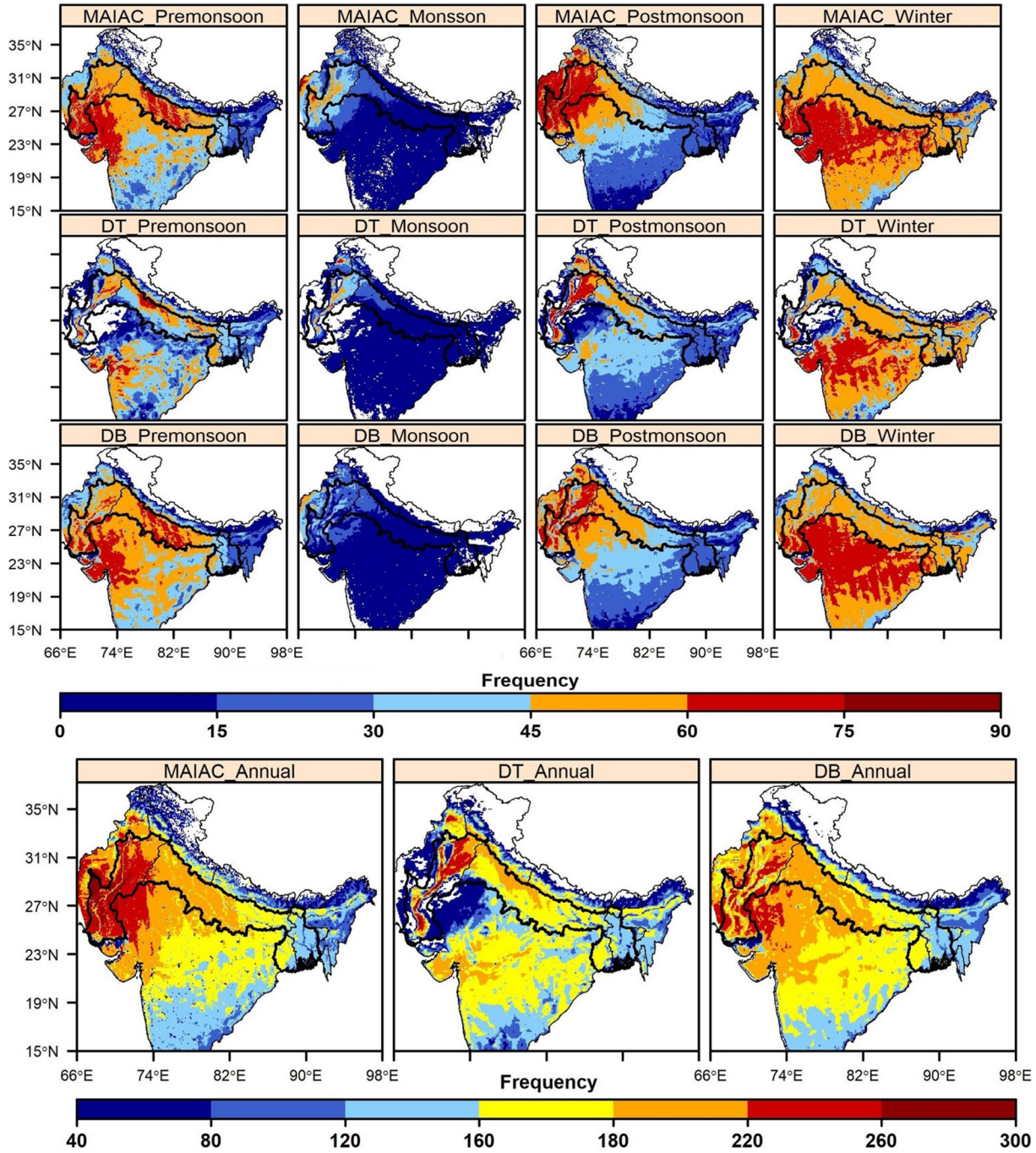

Fig. 4. Multiyear (2006–2016) seasonal and the annual AOD retrieval frequency over South Asia from different MODIS retrieval algorithms: MAIAC, DT and DB. The area demarcated by thick line is the IGP region.

Dhaka is a highly polluted city located in the lower part of IGP and is mainly affected by fine absorbing particles ($AOD_{AER} \sim 0.75$, AE: 1.18; Mhawish et al., 2017; Singh et al., 2017a, 2017b). The significant underestimated MAIAC AOD is primarily due to overestimated aerosol SSA.

Some inconsistencies (EE difference > 10%) were observed between MODIS Aqua and Terra retrieved AOD, at few AERONET stations, e.g. Karachi, Gual Pahari and Bhola (Table S3). The retrieval accuracy of Terra MAIAC was higher at the Bhola and Karachi AERONET stations, while Aqua showed better results in Jaipur. The aforementioned Terra-Aqua discrepancy is highest for DT, where the difference in EE retrieval accuracy exceeds 10% and the RMSE is > 0.03 in 10 AERONET stations. The Aqua and Terra DB remained most consistent, except in the Bhola and Kathmandu AERONET sites. The Terra-Aqua differences need further analysis on a case-by-case basis, which is beyond the scope of this manuscript.

Fig. 7 shows the retrieval bias, i.e. the deviation of the MODIS AOD retrieval from the AERONET AOD (AOD_{AER}). The AOD_{AER} was divided into bins of width of 0.1 and the retrieval bias was plotted as a function of the AOD. MAIAC AOD shows very low median bias and small quartile range at low AOD (< 0.5), with the bias taking negative values for higher AOD. For AOD > 0.5, the negative bias tends to be higher for Aqua than for Terra. The DT algorithm shows discrepancies in the retrieval bias between Aqua and Terra, with Terra DT AOD bias higher than Aqua DT AOD bias, especially for AOD > 0.5. The median DB AOD bias was negative at all aerosol loading conditions. For low AOD,

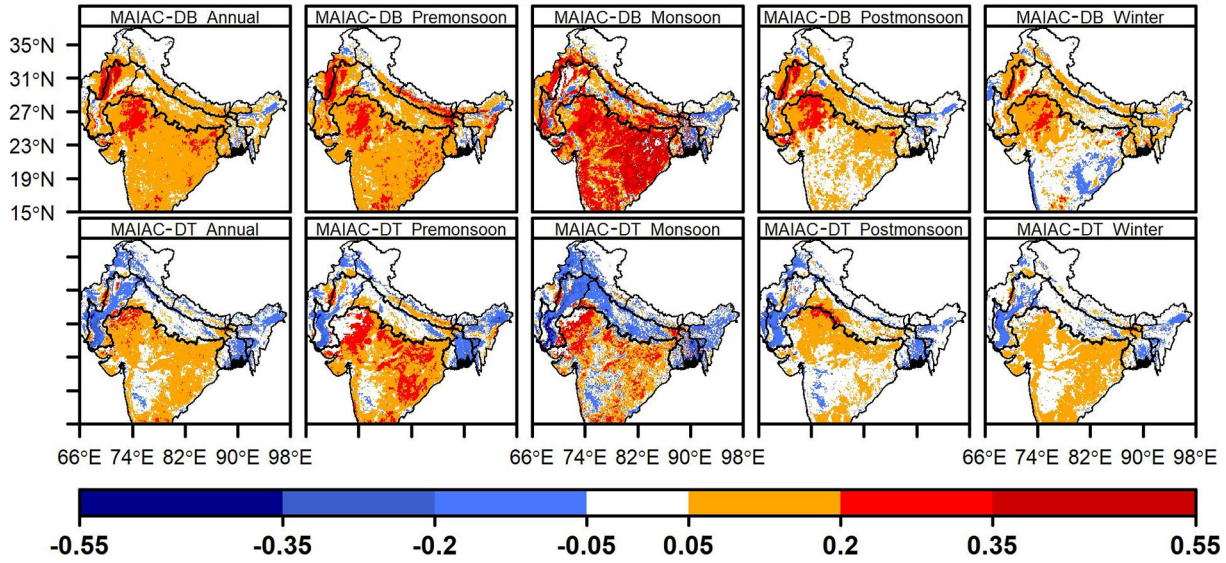

Fig. 5. Spatial distribution of multiyear (2006–2016) average differences of MAIAC and DB AOD (top row) and MAIAC and DT AOD (bottom row) AOD over South Asia. The thick black line represents IGP.

the DB negative bias was mainly associated with overestimation of the surface reflectance, which induce AOD underestimation. For higher aerosol loading, the assumptions related to the aerosol properties have a larger influence on the AOD retrieval accuracy over South Asia. The role of the surface cover and aerosol type on AOD retrieval for each algorithm are discussed in the following sections.

Fig. 8 shows the distribution of Terra and Aqua MODIS AOD bias with respect to AERONET AOD for all the matchup points per algorithm-pair over South Asia. We note that the mean bias for Terra tends toward more positive values compared to Aqua. Terra MODIS estimated higher AODs for all the algorithms (MAIAC: 6.03%, DT: 9.57%, DB: 6.36%) compared to Aqua MODIS AOD. The Terra-Aqua bias offset varied, with DT showing the highest offset (0.046) compared to MAIAC (0.024) and DB (0.023). A recent study by Gupta et al. (2018) also noted that Terra exhibited higher mean bias than Aqua. Furthermore, Sayer et al. (2015) noted small positive global-average offset

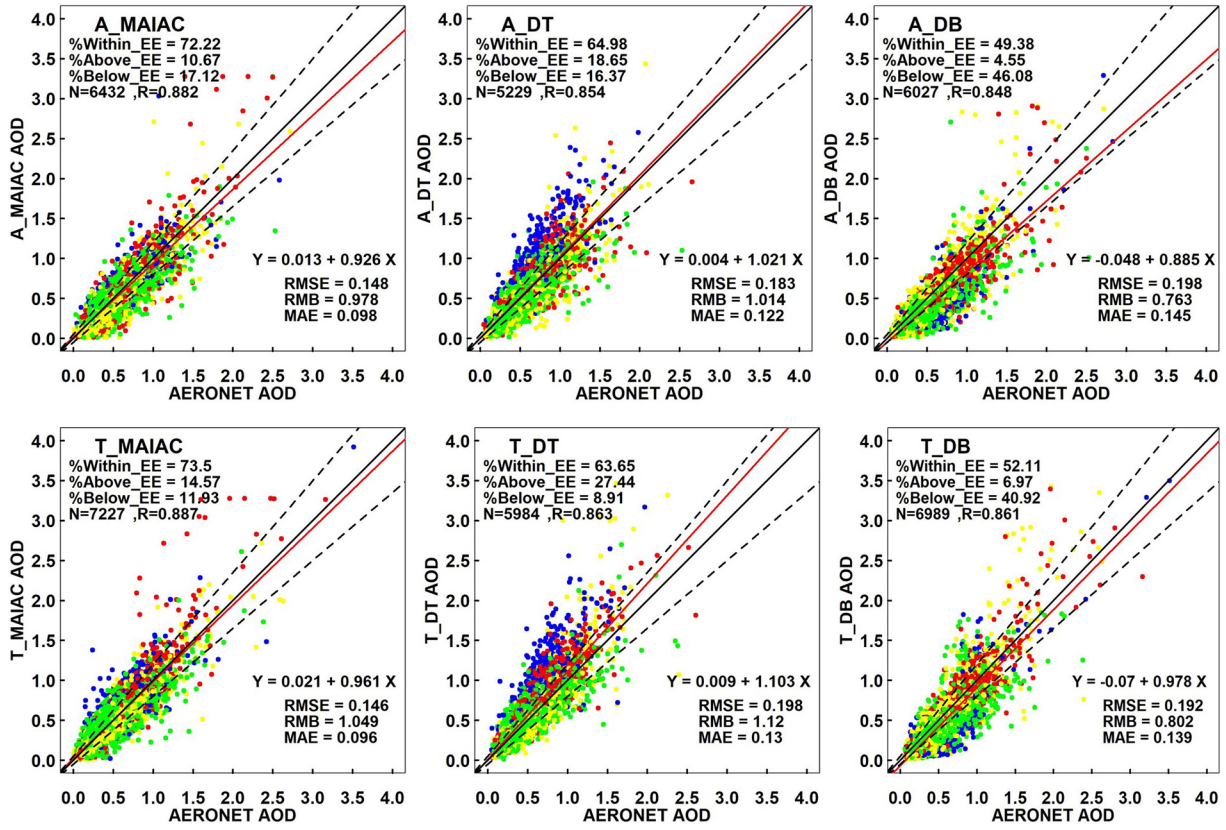

Fig. 6. Evaluation of Aqua and Terra MODIS MAIAC 1 km, DT 10 km and DB 10 km AOD against AERONET AOD (all sites across South Asia).
Note. The solid red line is the regression line, the dash lines are the EE boundaries, and the black solid line is the 1:1 line. (For interpretation of the references to color in this figure legend, the reader is referred to the web version of this article.)

Table 2
Error statistics of MODIS/AERONET comparison across South Asia.

Algorithm	N	AOD_{AE}	$AE_{440–870}$	R	RMSE	RMB	MAE	Within EE%	Above EE%	Below EE%
A_MAIAC	6432	0.477 ± 0.293	0.960 ± 0.420	0.882	0.148	0.978	0.098	72.22	10.67	17.12
A_DB	6027	0.498 ± 0.297	0.986 ± 0.401	0.848	0.198	0.763	0.145	49.38	4.55	46.08
A_DT	5229	0.507 ± 0.293	1.071 ± 0.364	0.854	0.183	1.014	0.122	64.98	18.65	16.37
T_MAIAC	7227	0.480 ± 0.290	0.986 ± 0.428	0.887	0.146	1.049	0.096	73.5	14.57	11.93
T_DB	6989	0.500 ± 0.301	1.003 ± 0.403	0.861	0.192	0.802	0.139	52.11	6.97	40.92
T_DT	5984	0.513 ± 0.288	1.077 ± 0.365	0.863	0.198	1.12	0.13	63.65	27.44	8.91

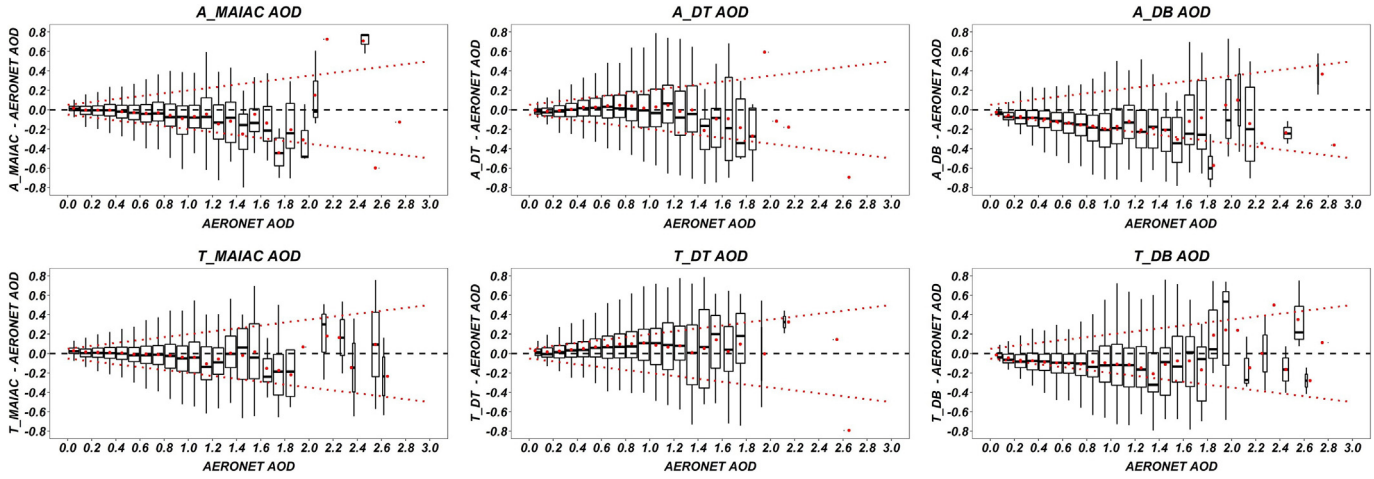

Fig. 7. Box plot of Aqua (A) and Terra (T) MODIS MAIAC 1 km, DT 10 km and DB 10 km AOD bias with respect to AERONET AOD (AOD_{AER}). The black horizontal dashed line represents zero bias and the red dotted lines represent the EE. For each box, the middle line, red dot, and upper and lower hinges represent the median, mean, and 25th and 75th percentiles, respectively. The whiskers extend to 1.5 times the interquartile range (IQR). (For interpretation of the references to color in this figure legend, the reader is referred to the web version of this article.)

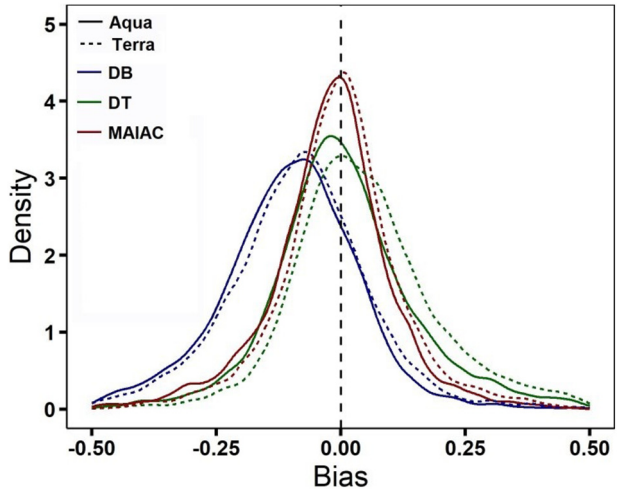

Fig. 8. Distribution of the Aqua and Terra MODIS MAIAC, DT and DB AOD bias over South Asia with respect to AERONET AOD.
Note. Solid curves: Aqua, dotted curves: Terra, vertical dashed line: zero bias.

between Terra and Aqua C6 DB AOD. The offset between the Terra and Aqua MODIS sensor might be due to various reasons including the instrument calibration, diurnal variability of the aerosols and of meteorological variables, unequal sampling of aerosol events across the region, and the diurnal cycle of cloud which tends to be higher in the afternoon compared to the morning (King et al., 2013). Moreover, the diurnal cycle of clouds affects also the number of matchups with AERONET, which we found to be higher by 12–14% for Terra than for Aqua (morning vs. afternoon). The variation of the mean bias offset between the algorithms is possibly tied to the assumptions about the aerosol properties, used by the retrieval algorithms (Levy et al., 2018).

3.2.2. Angular dependence of AOD retrieval

Satellite-based aerosol retrievals are commonly associated with multiple uncertainties of different magnitudes. Some potential errors are related to the satellite and solar geometries, while other are inherently linked to the surface characterization and aerosol type/model. Here, the influence of the viewing geometry, namely the viewing zenith angle (VZA), scattering angle (SA), and relative azimuth angle (RAA) on the bias in AOD retrieval was investigated. Each angle was binned into bin size of 10° independently, and the biases calculated for each bin averaged (Fig. 9). With reference to VZA, all the algorithms showed a larger number of matches at the edge of the scan, with most matchups between 40 and 60° (~54% of the total matchup points) and fewer matches at nadir (Fig. 9a, b). Moreover, all the algorithms showed only little dependence of the retrieval bias on the VZA, with a relatively constant positive offset bias (Terra - Aqua) at each VZA bin for each of the algorithms. Among the three algorithms, MAIAC appeared to have the lowest VZA dependence and the smallest bias. With increase in VZA (> 30°), both MAIAC and DT show VZA-AOD bias trend toward negative values while the DB bias remains negative with a negligible dependence on VZA. MAIAC showed lower negative mean bias (A: −0.019, T: −0.006) relative to DB (A: −0.111, T: −0.092), while DT showed comparable yet positive mean bias (A: 0.016, T: 0.066). Our findings agree with those reported over North America, where a trend of small negative retrieval bias with VZA was reported for DT and DB (Belle and Liu, 2016) and for MAIAC AOD (Superczynski et al., 2017).

The anisotropic properties of the surface reflectance affect the accuracy of AOD retrieval algorithms that use measurements from single view sun-synchronous orbit sensors, due to changes in the surface brightness in response to the view direction. For instance, the surface is generally brighter for backscattering geometry (RAA < 90°) than for

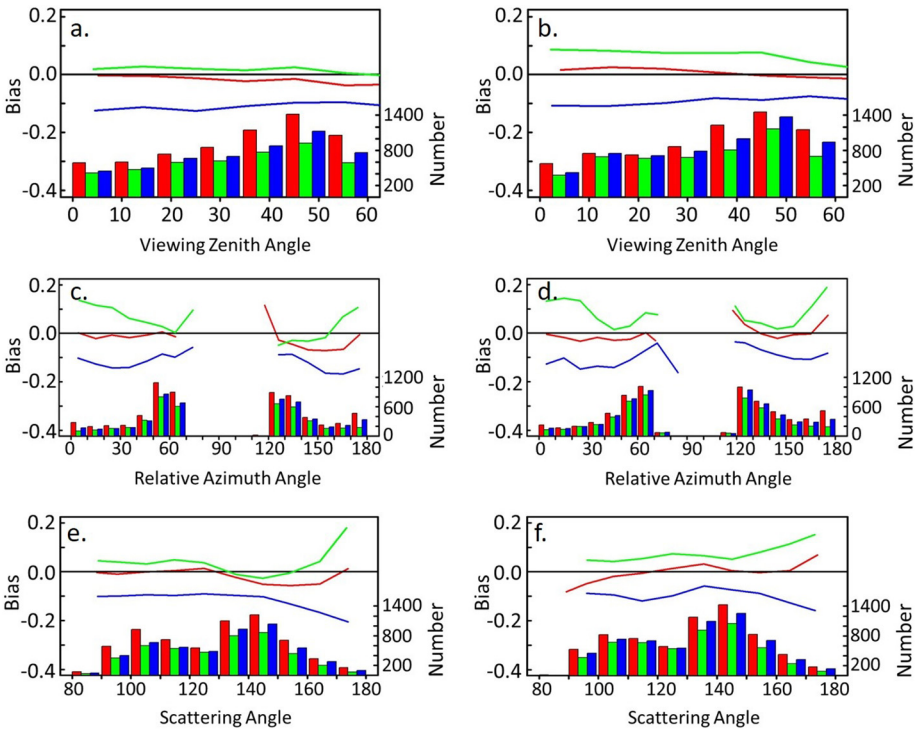

Fig. 9. Angular dependence of AOD retrieval bias of Aqua (a, c and e) and Terra (b, d and f) MAIAC (red), DT (green), and DB (blue) algorithms, on the Viewing Zenith Angle, Scattering angle, and Relative Azimuth Angle.
Note. The vertical bars represent the number of matchups in each angle bin. The horizontal black line represents the zero bias. (For interpretation of the references to color in this figure legend, the reader is referred to the web version of this article.)

forward scattering (RAA > 90°) (Roujean et al., 1992). By accounting for surface anisotropy (BRDF), MAIAC can potentially decrease the geometric dependence of the aerosol retrieval (Lyapustin et al., 2011b). Fig. 9 demonstrates that the number of matchups is not uniform for varying RAA, and that MAIAC, DT and DB all show a limited number of matches between 70 and 110° due to the limited MODIS orbital coverage (Superczynski et al., 2017). The bias in the forward scattering direction of the three algorithms, especially DT and DB, is more significant with the increase in the RAA. Similarly, in the backscattering direction, MAIAC shows little dependence on RAA and low bias (A, T: −0.01, −0.02) while larger biases are evident for DT (A, T: 0.07, 0.08) and DB (A, T: −0.11, −0.12).

The MODIS C6 algorithms show bias that varies also with the scattering angle. Both DT (0.05–0.20) and DB (−0.1 to −0.20) show relatively high biases, while MAIAC exhibits smaller bias (−0.09 to 0.05). Aqua MAIAC AOD shows almost zero bias for SA < 130°, and the bias tends to be negative at higher SA (SA > 130°: < −0.05). In contrast, Terra MAIAC AOD exhibits a varying bias pattern, with minimal values for 140° ≤ SA ≤ 160°. The SA bias dependency of DT and DB varies between Aqua and Terra, with relatively steady positive bias of DT for SA < 130° and increasing bias for SA > 130°, while the DB shows negative bias at all SA and the bias tends to be more negative at higher SA. The differences between Aqua and Terra could be attributed to several factors, as discussed above. In particular, one factor that affects the differences between Terra and Aqua retrievals is the diurnal variation of the aerosols. Observations from different SA influence the aerosol phase function, affecting the AOD retrieval (Levy et al., 2010; Sayer et al., 2015).

3.2.3. Aerosol size dependence of AOD retrieval

Assumptions related to the aerosol microphysical and optical properties often induce major uncertainties in the satellite retrieval of the TOA reflectance, especially for high aerosol loading conditions. The performances of all the MODIS algorithms were therefore evaluated against AERONET ground-truth observation by constraining the retrieval to three generic aerosol loading scenarios: (1) low AOD (≤0.2) conditions for which the contribution of the surface reflectance to the TOA signal is dominant, (2) moderate aerosol loading conditions (0.2 < AOD < 0.4) for which the TOA signal is influenced by both the surface reflectance and the aerosol, and (3) high AOD (≥0.4) conditions for which the contribution of the surface reflectance to the TOA signal is negligible and the uncertainty related to aerosol assumption is dominant (Sayer et al., 2014). Furthermore, considering AERONET AE as a first-order indicator of the optical dominance of fine-mode or coarse-mode aerosols, moderate to high AOD regimes (AOD > 0.2) were further classified into three aerosol sub-types: coarse particles (e.g. mineral dust, AE ≤ 0.7), mixed mode (a mixture of fine and coarse aerosols, 0.7 < AE < 1.3) and fine particles (e.g. mainly anthropogenic-like industrial emissions, biomass burning, etc., AE ≥ 1.3; Mhawish et al., 2017; Sayer et al., 2014). Initially, the MODIS AOD retrieval bias was plotted as a function of the AOD_{AER} and the particle size for all matchups points (Fig. 10), followed by considering only the collocated set of matchups (Table 3).

In Fig. 10, the $AE_{440–870}$ was binned into a bin size of 0.1, and the retrieval bias in each corresponding bin was plotted against the AE for AOD_{AER} < 0.2 (Fig. 10a) and AOD_{AER} > 0.2 (Fig. 10b). For low aerosol loading conditions (AOD_{AER} ≤ 0.2), the retrieval error that is attributed to the aerosol model is small compare to the contribution of the surface reflectance error, and the bias is relatively constant irrespective of the aerosol type. For low AOD (< 0.2), MAIAC had higher number of retrievals (A: 35–53%, T: 27%–60%) and a negligible mean bias (A,T: 0.001, 0.019) whereas DB underestimated the AOD (mean bias A, T: −0.054, −0.042) and DT had smaller absolute mean bias (A, T: −0.016, 0.019). All the algorithms showed offset between the Terra and Aqua MODIS instruments for AOD < 0.2, with the Terra data positively biased. For high AOD_{AER} (AOD_{AER} > 0.2) (Fig. 10b), the retrieval bias of all the algorithms was more dependent on the particle size, with MAIAC showing smaller mean retrieval bias: negative (A, T: −0.043, −0.011) when coarse aerosols were dominant and positive (A, T: 0.018, 0.033) when fine aerosols dominated. The same bias pattern was also observed for DB (A, T: −0.145, −0.124; coarse aerosol and A, T: −0.068, −0.048; fine aerosol) while DT showed an opposite pattern, with a positive mean bias (A, T: 0.076, 0.112) for coarse aerosols and a smaller bias (A, T: −0.009, 0.041) for fine aerosols.

To compare the performance of the three algorithms under identical atmospheric conditions, only collocated matchups were considered,

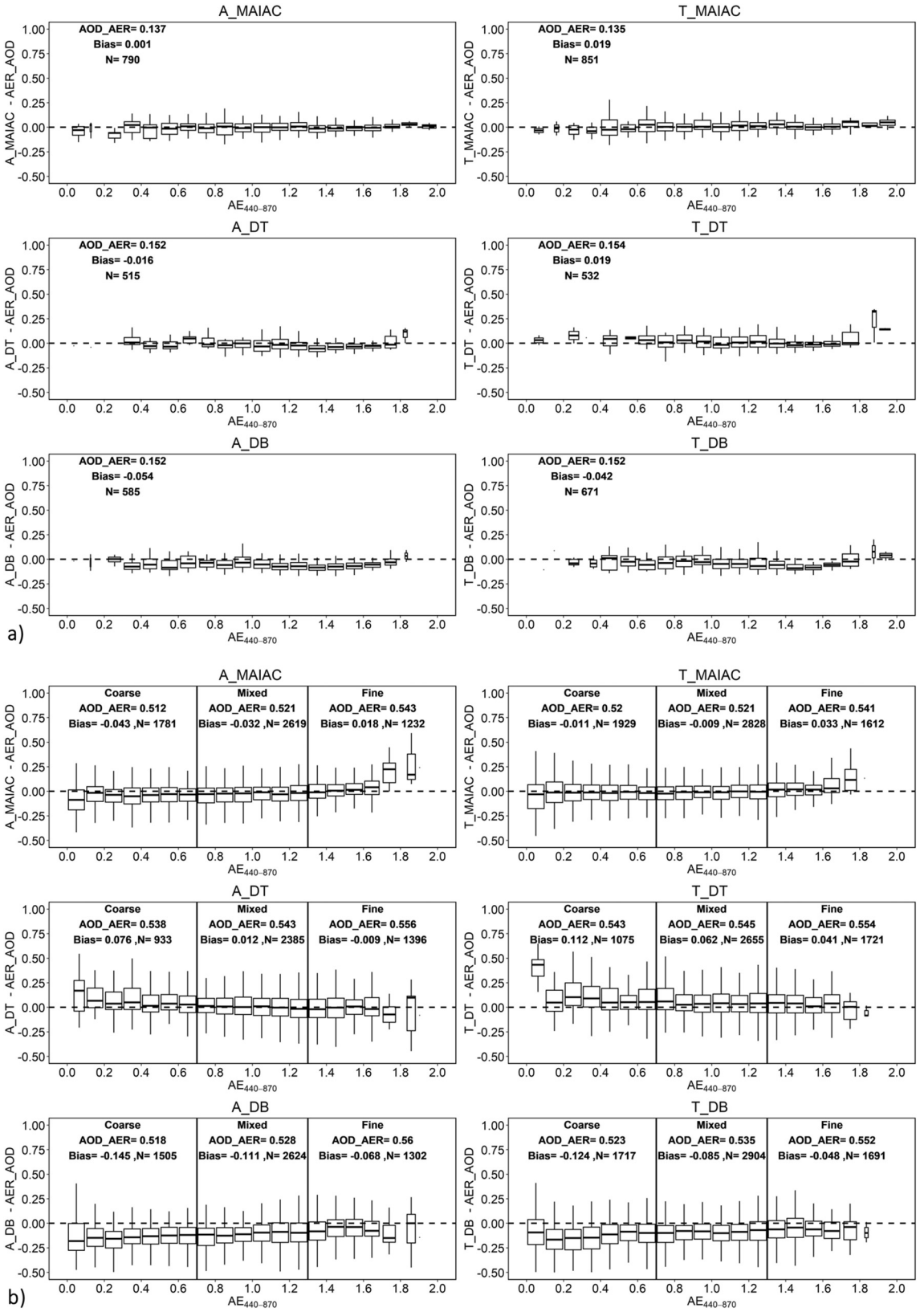

Fig. 10. Variation of the retrieval bias as a function of the Angstrom Exponent (AE) (a) for AERONET AOD < 0.2, (b) for AERONET AOD > 0.2.
Note: The black horizontal dashed line represents zero bias. The black vertical solid lines separate the coarse (AE < 0.7), mixed (0.7 < AE < 1.3) and fine (AE > 1.3) aerosol fractions. AOD_AER represents the mean AERONET AOD, the bias represents the mean bias (Σ (MODIS AOD − AERONET AOD) / N), and the N represents number of matchup points.

Table 3
Error statistics of MODIS/AERONET comparison of AOD at 550 nm for collocated observations stratified by aerosol loading and size. The best performing algorithm by each metric in indicated in bold.

AOD	$AE_{440–870}$	N	R			EE			RMSE			RMB		
			MAIAC	DT	DB	MAIAC	DT	DB	MAIAC	DT	DB	MAIAC	DT	DB
< 0.2	–	440 (A)	0.467	**0.474**	0.348	**78.18**	73.41	45.45	**0.063**	0.070	0.087	**1.032**	0.838	0.602
		457 (T)	**0.472**	0.405	0.298	**78.77**	78.34	42.67	**0.070**	0.077	0.089	1.136	**1.070**	0.660
≥0.2, < 0.4	Coarse	247 (A)	0.488	**0.540**	0.378	**77.73**	74.49	53.44	**0.085**	0.094	0.129	1.046	**1.017**	0.721
		270 (T)	0.518	**0.541**	0.428	**74.44**	69.63	54.44	**0.089**	0.113	0.140	**1.074**	1.131	0.753
	Mixed	778 (A)	0.509	**0.519**	0.431	**78.92**	70.44	53.86	**0.088**	0.098	0.125	**1.027**	0.973	0.749
		900 (T)	0.464	**0.479**	0.431	**77.67**	66.78	54.78	**0.088**	0.106	0.124	**1.057**	1.102	0.757
	Fine	389 (A)	**0.634**	0.604	0.531	**80.21**	61.95	47.81	**0.082**	0.103	0.120	**1.044**	0.966	0.796
		539 (T)	**0.616**	0.589	0.559	**82.37**	65.31	48.79	**0.079**	0.101	0.121	**1.066**	1.070	0.785
≥0.4	Coarse	459 (A)	0.741	**0.745**	0.671	**78.43**	69.93	44.23	**0.141**	0.168	0.224	**0.923**	1.101	0.725
		605 (T)	0.717	**0.725**	0.643	**78.51**	61.65	47.77	**0.147**	0.218	0.235	**0.954**	1.152	0.743
	Mixed	1051 (A)	**0.827**	0.807	0.791	**72.41**	65.56	54.04	**0.160**	0.191	0.217	0.938	**1.014**	0.800
		1272 (T)	**0.837**	0.831	0.822	**73.82**	63.44	56.76	**0.159**	0.210	0.204	**0.964**	1.090	0.837
	Fine	606 (A)	**0.842**	0.749	0.754	**77.89**	62.87	64.19	**0.158**	0.194	0.202	**1.015**	1.026	0.899
		864 (T)	**0.856**	0.808	0.796	**75.35**	64.47	64.12	**0.166**	0.180	0.186	**1.038**	1.076	0.918
All AOD	–	3970 (A)	**0.891**	0.876	0.851	**76.95**	67.68	52.82	**0.126**	0.151	0.176	0.993	**0.994**	0.769
		4907 (T)	**0.889**	0.880	0.858	**76.81**	65.95	54.27	**0.131**	0.166	0.173	**1.026**	1.096	0.798

resulting in 3970 and 4907 data points for Aqua (A) and Terra (T), respectively (Table 3). The error statistics of the different algorithms is almost similar for any given AOD-AE stratification. For low aerosol loading conditions ($AOD_{AER} \leq 0.2$), only MAIAC and DT algorithms achieved satisfactory retrieval accuracy (EE: 73.4–78.8%). MAIAC and Terra DT slightly overestimated the AOD (RMB: 1.032–1.136) while the Aqua DT underestimated the AOD (RMB: 0.838). The DB algorithm significantly underestimated the AOD (RMB: A, T: 0.602, 0.660), suggesting that the surface reflectance (of the dark surfaces) is overestimated.

For moderate to high aerosol loading conditions, MAIAC retrievals were less influenced by the aerosol climatology, achieving satisfactory retrieval (EE A, T: 72.4–82.4%), small bias (RMB A, T: 0.923–1.074) and low RMSE (A, T: 0.079–0.166). The error statistics clearly indicate MAIAC's small dependence on the particle size, and its superior ability to retrieve AOD under diverse aerosol loading conditions. Under the same scenarios for coarse aerosol, the relative mean bias remains ≥1 for DT and < 1 for DB, indicating over- and under retrievals of AOD. The DT is less sensitive to the aerosol type and its performance in retrieving coarse and mixed aerosols is good. In contrast, DB is more sensitive to the particle size and obtained the highest accuracy in retrieving fine aerosols. For AOD > 0.4, the DB obtained more AOD retrievals that fell within the EE for fine aerosol (EE A, T: 64.19%, 64.12%) compared to coarse aerosols (EE A, T: 44.23%, 47.77%, Table 3).

3.3. Surface cover dependence of the retrieval accuracy

Retrieving aerosols over heterogeneous land surfaces is often challenging, since minor errors in the surface reflectance estimates may induce large deviations in the AOD retrieval, especially for low aerosol loading conditions (Levy et al., 2007). To address the vast and complex land-use pattern of South Asia, the sensitivity of the MODIS aerosol retrieval algorithms on the surface reflectance was investigated under different aerosol loading scenarios. An eight-day composite MAIAC Normalized Difference Vegetation Index (NDVI) was interpolated using spline interpolation to estimate the daily NDVI. The performance of the algorithms was evaluated both for $AOD_{AER} \leq 0.2$ and $AOD_{AER} > 0.2$, with the surface type classified into four classes: arid surfaces (NDVI ≤ 0.2), light/-sparse vegetation (0.2 < NDVI < 0.4), moderate vegetation cover (0.4 ≤ NDVI < 0.6), and dense vegetation cover (NDVI ≥ 0.6).

Table 4 presents the distribution of the retrieval errors as a function of NDVI which is used as a proxy of the surface cover types. For $AOD_{AER} \leq 0.2$, with the increase in surface vegetation coverage, the retrieval accuracy of both Aqua and Terra MAIAC increases consistently, and registers the highest number of retrievals in most conditions. The numbers of MAIAC AOD retrievals within the EE increased by 16% with the increase in the vegetation cover. Similarly, the DT AOD was most accurate over densely vegetated surfaces. As shown in Table 4, both the MAIAC (EE: 86.3–89.9%) and DT (EE: 79.4–86.1%) algorithms showed enhanced retrieval accuracy over dark vegetated surfaces (NDVI > 0.6) for AOD < 0.2, indicating accurate estimation of the surface reflectance. Over dry surfaces (NDVI < 0.2), MAIAC outperformed the DB and DT algorithms in the number of matchup points, yet all the algorithms passed the EE retrieval threshold (67%). In particular, poor retrieval accuracy was noted for DB, with the best accuracy obtained over arid areas (NDVI < 0.2), EE: 68.2–73.3%. The reduced accuracy (underestimation of AOD) for higher NDVI (NDVI > 0.2), EE: 30.0–59.0%, suggests overestimation of surface reflectance for dark/vegetated surfaces.

For $AOD_{AER} > 0.2$, accurate estimation of the aerosol optical properties has a greater impact on AOD retrieval accuracy. MAIAC showed a higher retrieval accuracy for higher NDVI, with increasing number of matchup points within the EE interval. This indicates good estimation of the aerosol optical properties along with the surface reflectance over dark/vegetated surfaces, leading to accurate AOD retrieval. The MAIAC AOD retrieval accuracy over dark surfaces is attributed to the spectral similarity of the BRF shape between the blue and SWIR (2.1 μm) bands, an assumption that works well over dark surfaces and leads to improved estimates of the surface reflectance and of the aerosol optical properties (Lyapustin et al., 2011b). The MODIS DT showed a higher AOD retrieval accuracy (EE: ~78%) over densely vegetated surfaces (NDVI > 0.6) than over sparsely and moderately vegetated areas (EE: 60.0–63.4%). The DB algorithm showed constant error in AOD retrieval for NDVI > 0.2 (EE: 49.7–56.7%). Over arid region (NDVI < 0.2), the DB algorithm significantly underestimated AOD for AOD > 0.2 but was more accurate for AOD < 0.2 conditions, indicating that the retrieval error is related mostly to the assumptions regarding the aerosol optical properties. Coarse aerosols are common over arid regions but the DB algorithm showed a significant underestimation of the AOD when the NDVI < 0.2 (see Section 3.2).

3.4. Seasonal variability of the retrieval accuracy

Previously, strong seasonality has been noted in the performance of Aqua MODIS products (DT, DB and the merge DT-DB; Mhawish et al., 2017), which instigated us to examine the seasonality of MAIAC AOD

Table 4
Error statistics of MODIS/AERONET comparison of AOD at 550 nm stratified by MAIAC NDVI.

AOD_{AE}	NDVI	MAIAC					DT					DB				
		N	R	RMSE	RMB	EE	N	R	RMSE	RMB	EE	N	R	RMSE	RMB	EE
AOD < 0.2	NDVI < 0.2	**A: 256**	**0.456**	**0.066**	**1.152**	70.31	12	0.089	0.066	1.208	**75.00**	66	0.182	0.065	0.875	68.18
		T: 331	0.550	**0.059**	1.473	73.11	33	**0.594**	0.060	1.256	**78.79**	146	0.246	0.065	**0.929**	73.29
	0.2 < NDVI < 0.4	**A: 253**	0.352	0.077	1.241	70.36	155	**0.426**	**0.070**	**1.059**	**76.13**	190	0.242	0.075	0.802	58.95
		T: 261	**0.316**	**0.099**	1.401	63.98	161	0.212	0.119	1.362	**67.08**	196	0.247	0.081	**0.864**	55.10
	0.4 < NDVI < 0.6	A: 100	**0.483**	**0.063**	**0.989**	**81.00**	183	0.362	0.082	0.789	68.85	**191**	0.321	0.095	0.553	37.70
		T: 110	**0.332**	**0.085**	1.123	**84.55**	201	0.302	0.085	**0.992**	76.12	**207**	0.214	0.098	0.587	29.95
	NDVI > 0.6	**A: 182**	**0.499**	**0.056**	**0.924**	**86.26**	165	0.485	0.056	0.844	79.39	139	0.416	0.089	0.461	41.01
		T: 149	**0.532**	**0.058**	**1.001**	**89.93**	137	0.531	0.059	1.066	86.13	122	0.390	0.081	0.518	53.28
AOD > 0.2	NDVI < 0.2	**A: 1015**	0.832	**0.165**	0.780	57.54	97	**0.856**	0.175	**1.025**	**57.73**	535	0.857	0.216	0.611	24.67
		T: 929	0.866	**0.136**	**0.861**	**67.60**	181	**0.937**	0.184	1.185	62.43	677	0.869	0.217	0.612	30.28
	0.2 < NDVI < 0.4	**A: 3199**	**0.848**	**0.158**	**1.009**	**71.80**	2592	0.822	0.202	1.082	63.43	3140	0.818	0.213	0.810	52.39
		T: 3698	**0.835**	**0.159**	**1.055**	**70.77**	2992	0.828	0.223	1.082	59.99	3494	0.835	0.198	0.810	56.70
	0.4 < NDVI < 0.6	A: 949	**0.904**	**0.167**	**0.981**	**79.35**	**1544**	0.834	0.188	0.948	60.56	1406	0.843	0.198	0.768	51.92
		T: 1170	**0.916**	**0.161**	**1.008**	**80.00**	**1748**	0.859	0.190	0.806	62.01	1708	0.862	0.202	0.806	52.46
	NDVI > 0.6	**A: 478**	**0.923**	**0.090**	**0.970**	**86.82**	481	0.876	0.137	0.981	78.79	360	0.906	0.156	0.740	50.83
		T: 579	**0.913**	**0.116**	**0.993**	**85.49**	531	0.896	0.151	1.067	77.59	439	0.876	0.182	0.761	49.66

Note: In each row, the best performing algorithms by each metric in indicated in bold. Within each cell, the upper value is for Aqua while the lower one is for Terra.

(Fig. 11, Table S4). As discussed in the previous sections, the retrieval accuracy of the three algorithms depends on the aerosol type, which may vary spatially and temporally and is associated with different emission sources. Fig. S2 shows the seasonal variation of the aerosol optical properties across South Asia, using daily mean AERONET products. The $AE_{440–870}$ was used to assess the dominant aerosol size mode, and the spectral dependence of the SSA was used to differentiate among absorbing and non-absorbing aerosols. The CWV was used as a proxy of humidity to examine the impact of humidity on the aerosol optical properties.

A notable spatial and temporal variation of the aerosol properties and AOD values have been observed over South Asia, with all stations showing decreasing AE values during premonsoon and monsoon, suggesting the dominance of coarse aerosols. The upper IGP stations (Karachi, Lahore and Jaipur) exhibited the highest AOD retrieval during monsoon, as well as lower AE due to particle hygroscopic growth (Fig. S2). The larger particle size and their moisture content result in enhanced spectral variation of the SSA, and translates into a higher AOD. In the middle IGP (Gual Pahari, Kanpur and Gandhi college), the AOD decreased with the fraction of the coarse particles and mixed type aerosols prevailed. Although the CWV did not show significant spatial variability in the monsoon season, the particle size distribution and the AOD varied significantly, most probably due to the variation in aerosol hygroscopicity and mixing state (i.e. composition) across the region (Wang and Martin, 2007). The upper IGP AERONET stations are located near the coast and are more affected by sea salt, which is known to grow hygroscopically (Kumar et al., 2018). In the middle and lower IGP, particles do not grow much hygroscopically, due to wet deposition. Similarly, in the lower IGP stations (Dhaka and Bhola) lower AOD was retrieved and the aerosol had a higher contribution of fine particles. The spectral dependence of the SSA had a slight negative slope, indicating that the contribution of scattering and absorbing aerosols is comparable. During the winter and postmonsoon seasons, all the AERONET stations except those in the arid regions (Jaipur and Karachi) experienced predominantly fine absorbing aerosols.

In general, the coarse aerosol fraction tends to decrease from west to east and attains the highest values over dust-laden arid areas (e.g. Karachi and Jaipur). The positive wavelength dependency of the SSA decreases from west to east and tends to be negative for absorbing

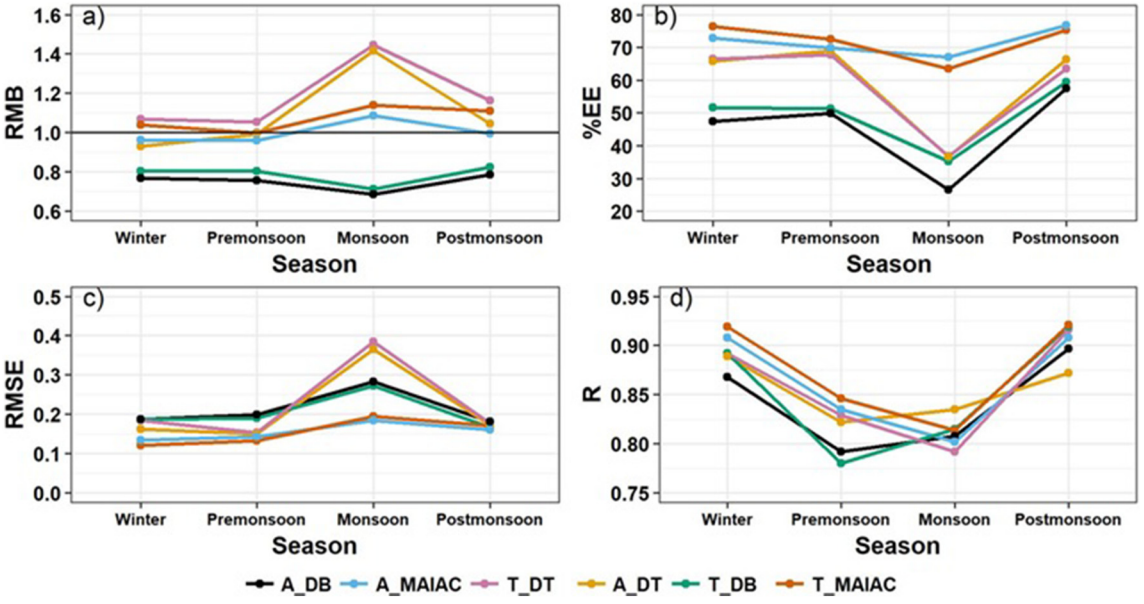

Fig. 11. Seasonal variation of error statistics of MODIS/AERONET comparison of AOD at 550 nm.

aerosols in the east. In Northern IGP (Lumbini, Pokhara, Kathmandu and Jomsom), no significant variation of aerosol properties was evident. Temporally, during the monsoon and premonsoon periods higher fractions of coarse particles are experienced over South Asia relative to the winter and postmonsoon, which are dominated by fine particles.

The spatial and temporal variation of the aerosol types influences the aerosol retrieval accuracy. During monsoon, the relative humidity is high, resulting in large particle sizes and higher SSA (Wang and Martin, 2007). The three MODIS algorithms show higher uncertainty and smaller number of matchup points due to higher cloud cover. The varying uncertainty in retrieving AOD among the MODIS algorithms is due to the different assumptions about the aerosol optical and microphysical properties. Terra and Aqua MAIAC show a higher number of matchup points (22–33%) (Table S4) and a lower retrieval bias (RMB; A, T: 1.088, 1.14) (Fig. 11a) in the monsoon season, compared to the other algorithm that obtain smaller number of retrievals and a higher RMB from the AERONET AOD (28.8–44.6%), suggesting that the MAIAC dynamic aerosol model accounts better for hygroscopic growth of aerosol particles, leading to more accurate AOD retrievals. The number of matchup points of the MAIAC/AERONET AOD that fell within the EE was higher than those of DT (A: 36%, T: 27%) and DB (A: 41%, T: 28%) (Fig. 11b).MAIAC also has lower RMSE (Fig. 11c). The highest DT/DB disagreement in the retrieval accuracy was observed during the monsoon season, due to the algorithmic discrepancies regarding the effect of ambient moisture on the aerosol particles (i.e. hygroscopic growth). Specifically, the DT algorithm assumes higher absorbance (lower SSA) of coarse particles (i.e. dust), which leads to AOD overestimation when hygroscopic growth takes place. On the other hand, overestimation of the SSA by the DB algorithm leads to AOD underestimation.

3.5. MAIAC aerosol model

MAIAC uses three aerosol models, two for generic absorbing aerosols e.g. coarse (dust) and fine (smoke), and one for less absorbing aerosols (background) that are prescribed in each region individually (Lyapustin et al., 2011b). MAIAC classifies aerosols into smoke or dust based on short wavelength absorption and the effective particle size (Lyapustin et al., 2012). The absorption (i.e. estimated imaginary refractive index) of brown carbon (in smoke) and iron compounds (in dust) is enhanced for short wavelengths. Thus, for absorbing ambient aerosols, the aerosol reflectance at 0.412 μm would be lower than that predicted from the 0.466 μm and 0.646 μm channels. Initially aerosol reflectance is calculated and evaluated using AOD that is retrieved by the background aerosol model and a known spectral surface BRDF. Next, using a power law spectral dependence, the Angstrom exponent is derived and the absorption parameter is measured as the ratio of measured to predicted aerosol reflectance at 0.412 μm. For the absorbing aerosol types (lower absorption parameter), the smoke/dust tests are further implemented to classify the absorbing aerosols into smoke or dust aerosol (Lyapustin et al., 2012, 2018). Considering the extreme diverse aerosol types across South Asia, the sensitivity and retrieval accuracy of MAIAC in detecting dust and smoke has been evaluated by taking into account the aerosol size, absorbing behavior and loading parameters (AE, SSA and AOD) retrieved from the AERONET. Namely, the MODIS-AERONET collocated dataset was divided into three subsets based on the detected MAIAC aerosol type: Dust (A: 132, T: 66), Smoke (A: 932, T: 966) and Background (A: 5368, T: 6195). Overall, all MAIAC aerosol types showed good agreement with AERONET (R: 0.841–0.890; RMSE: 0.135–0.279; Table 5). However, for the detected smoke events MAIAC AOD showed a slightly positive bias (RMB; A, T: 1.049, 1.051) whereas for dust events it significantly underestimated AOD (RMB; A, T: 0.866, 0.938) indicating lower absorbing dust in the assumed model.

Due to transboundary transport of aerosols, dust particles are often mixed with urban aerosols (Kumar et al., 2017; Sen et al., 2017), which subsequently change the spectral behavior of the SSA relative to pure mineral dust (Russell et al., 2014). The performance of the MAIAC algorithm in detecting dust and smoke aerosols has been examined as a function of the particle size, utilizing AERONET $AE_{440–870}$, and the particle absorbing properties, using AERONET SSA_{440} (Fig.12). Most of the detected dust showed lower SSA_{440}, ranging between 0.85 and 0.95, with the $AE_{440–870}$ varying between 0.0 and 0.8. However, the overall number of dust events was low, in part due to the low sensitivity of MAIAC to detect low airborne dust loading (AOD $<$ 0.4). Surprisingly, larger fractions of dust were detected over Kanpur (number of dust events - A: 47, T: 30) and Gandhi college (A: 25, T: 18) compared to Jaipur (A: 15, T: 3). This may indicate the lower sensitivity of MAIAC to detect dust over bright surfaces. As for smoke events, MAIAC AOD showed good agreement with AERONET AOD, with very large number of retrievals within the EE (75–77.5%). Indeed, Table 5 clearly indicates that MAIAC has a higher sensitivity for detection of smoke than dust, and that it is able to detect smoke at AOD $>$ 0.3. For most of the detected smoke events, the $AE_{440–870}$ varied between 0.2 and 1.5, with approximately 93% of the total detected smoke events showing SSA_{440} $<$ 0.93 (both Aqua and Terra). As for the 7% of the smoke events with SSA_{440} $>$ 0.93, 62–76% of these cases showed decreasing spectral SSA with increasing wavelength, indicating the presence of absorbing aerosols from smoldering rather than flaming sources (Reid et al., 2005) and mixed state aerosols (Wang and Martin, 2007). Overall, MAIAC is capable of distinguishing absorbing from non-absorbing aerosols, and has higher sensitivity in discriminating the particle size. Although only minor variation between Terra and Aqua were observed regarding the aerosol model selection, Terra MAIAC has shown a higher skill in retrieving smoke at low AE conditions. In days where both dust and smoke aerosols were not detected, the regional aerosol model of MAIAC (i.e. the background model) performed well and was satisfactory, with $>$ 71% of retrievals within the EE.

4. Conclusions

This study presents a comprehensive evaluation of the new MAIAC retrieval algorithm over South Asia for the years 2006–2016. We compared MAIAC with the two operational MODIS C6 AOD retrieval algorithms: DT and DB, and against AERONET AOD. Moreover, we examined the consistency between the Terra and Aqua MODIS sensors over South Asia. We utilized a 3×3 pixel window, which gives a $3 \times 3\,km^2$ averaging area for MAIAC, and $30 \times 30\,km^2$ area (at nadir) for DT and DB retrievals centered around each AERONET station, using a time window of $\pm$ 60 min around the satellite overpass time. The retrieval accuracy was assessed under varying aerosol loading, aerosol types, surface cover, viewing geometry, and seasonality. The model performance was assessed using RMSE, MAE, RMB and the percentage of retrievals falling within the EE.

A robust accuracy assessment of MAIAC, DT and DB AOD against AERONET AOD indicated the superiority of MAIAC in terms of the number of valid high-quality retrievals and the retrieval accuracy in terms of the fraction falling within the EE. The MAIAC AOD showed a very low median bias at low AOD, which with the increase in aerosol loading appears to be negative (especially for Aqua). MAIAC was also able to generate a richer spatial AOD pattern over varied surfaces and showed higher capability to capture fine scale features such as wildfire smoke plumes, haze, and dust. MAIAC was also obtained in between clouds and snow patches, which tend to restrict the retrieval of the other operational MODIS algorithms. We found that Terra MODIS retrieved higher AOD than Aqua MODIS, with a larger difference by the DT algorithm (9.57%) than by MAIAC (6.03%) and DB (6.36%). The mean bias between Terra MODIS AOD and AERONET AOD was more positive than that of Aqua AOD, and the offset of the mean bias was higher for DT (0.05) than for MAIAC and DB (0.02).

In terms of the VZA, the viewing geometry dependence of the bias was lowest for MAIAC. This finding also holds true for the RAA and SA.

Table 5
Error statistics of MODIS/AERONET comparison of AOD at 0.55 μm, stratified according to the MAIAC aerosol model.

Aerosol model	N	R	RMSE	RMB	MAE	Within EE%	Above EE%	Below EE%
Background	A: 5368	0.878	0.137	0.968	0.092	71.85	10.23	17.92
	T: 6195	0.890	0.135	1.05	0.091	73.56	14.43	12.01
Dust	A: 132	0.841	0.250	0.866	0.203	50.00	7.58	42.42
	T: 66	0.870	0.279	0.938	0.215	46.97	10.61	42.42
Smoke	A: 932	0.868	0.187	1.049	0.112	77.47	13.63	8.91
	T: 966	0.844	0.197	1.051	0.118	74.95	15.73	9.32

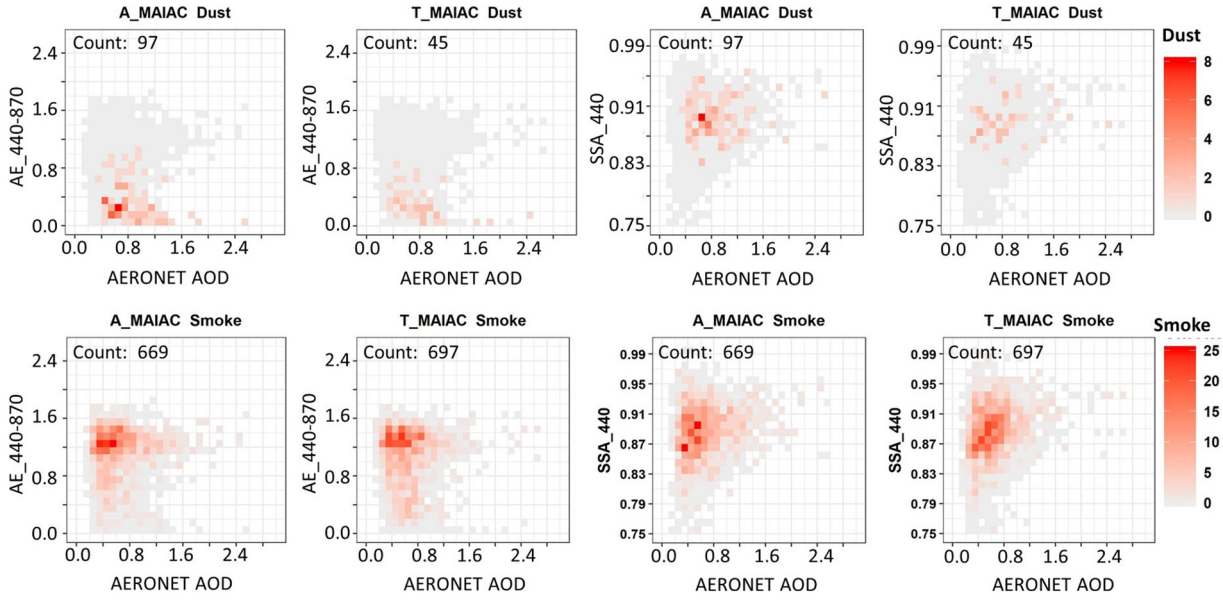

Fig. 12. Frequency distribution of MAIAC detected dust and smoke events as a function of AERONET AE, SSA and AOD over South Asia.

Interestingly, the inconsistency between Aqua and Terra MODIS in the SA dependence was noted for all the algorithms, possibly reflecting the local diurnal variation of the aerosol type, surface reflectance, or the atmospheric column properties (e.g. moisture profile). The AOD retrieval accuracy of MAIAC was analyzed as a function of the surface cover, with MAIAC showing a higher retrieval accuracy over all surface types compared to DT and DB. For AOD ≤ 0.2, both MAIAC and DT were more accurate in estimating the surface reflectance, whereas a gradual decrease in the retrieval accuracy was noted for DB. For AOD > 0.2, MAIAC showed a higher retrieval accuracy for a corresponding increase in the NDVI.

Considering the diversity and magnitude of the aerosol loading over South Asia, the retrieval accuracy was also assessed for three aerosol loadings and types. We found minor influence of the aerosol type on the MAIAC retrieval accuracy for $AOD_{AER} \leq 0.2$ but the relative bias increased gradually with the increase in aerosol load. For collocated observations, MAIAC achieved satisfactory retrieval accuracy at low AOD, showing a slight positive bias. Similar performance was also observed under moderate to high aerosol loading conditions, asserting its superiority in retrieving AOD for diverse aerosol scenarios. In contrast, the DT algorithm was less sensitive to the aerosol type and performed very well in retrieving coarse and mixed-type aerosols. The DB algorithm showed higher dependence on the aerosol type, performing best in retrieving fine mode aerosols.

The seasonal variation of the retrieval accuracy of the MODIS algorithms is governed strongly by dominant aerosol type, surface brightness, and meteorological variables. The accuracy of the AOD retrievals in the monsoon season is significantly lower when applying the DT and DB algorithms rather the MAIAC algorithm. Both the DT and DB algorithm assumptions failed in treating hygroscopic growth of aerosol particles during monsoon, compared to the MAIAC algorithm, which showed higher AOD retrievals falling within the EE by (26.58–40.57%). In other seasons, the retrieval accuracy of all algorithms was better but MAIAC outperformed the other algorithms.

The three MAIAC aerosol models showed good agreement with the AERONET aerosol types, in particular in distinguishing absorbing and non-absorbing aerosols. Specifically, the smoke model performed particularly well with almost a neutral bias, while the dust model significantly underestimated the AOD due to higher absorbing dust aerosols than assumed in the aerosol model. The lower sensitivity of MAIAC dust model to detect dust over bright surfaces was noted especially in Karachi and Jaipur.

To conclude, we found that MAIAC has superior capabilities to retrieve AOD over diverse surfaces, varying viewing geometry and diverse aerosol types over South Asia, showing better spatial coverage and smaller bias than DT and DB algorithms when compared to the AERONET ground-truth. MAIAC's consistent ability to provide AOD at 1 km resolution opens new perspectives in aerosol related research over the South Asia, especially for epidemiological and climatological studies.

Acknowledgements

The research is supported by India-Israel bilateral research project funded by University Grants Commission to T.B. (Grant No. 6-11/ 2018 IC) and Israel Science Foundation to D.B. (0472714). A.M. acknowledges the Jawaharlal Nehru Scholarship from Jawaharlal Nehru Memorial Fund (JNMF), New Delhi for Doctoral studies. Authors also thank Yujie Wang, University of Maryland for providing MAIAC data, Michael Dorman, Hebrew University of Jerusalem for help in data processing, and anonymous reviewers and associate editor Prof. P Yang for their constructive comments on the draft manuscript.

Data availability

The MODIS data used in this study are available at Atmosphere Archive & Distribution System (LAADS) (https://ladsweb.nascom.nasa.gov/search/), and the AERONET products at https://aeronet.gsfc.nasa.gov/. We would like to thank the Principal Investigators for establishing and maintaining AERONET sites. The authors are very thankful for the anonymous reviewers and the editor for their constructive comments on the manuscript.

Appendix A. Supplementary data

Supplementary data to this article can be found online at https://doi.org/10.1016/j.rse.2019.01.033.

References

Altaratz, O., Bar-Or, R.Z., Wollner, U., Koren, I., 2013. Relative humidity and its effect on aerosol optical depth in the vicinity of convective clouds. Environ. Res. Lett. 8 (3), 034025.

Banerjee, T., Murari, V., Kumar, M., Raju, M.P., 2015. Source apportionment of airborne particulates through receptor modeling: Indian scenario. Atmos. Res. 164, 167–187.

Banerjee, T., Kumar, M., Mall, R.K., Singh, R.S., 2017. Airing 'clean airing' clean India mission. Environ. Sci. Pollut. Res. 24 (7), 6399–6413.

Banerjee, T., Kumar, M., Singh, N., 2018. Aerosol, climate, and sustainability. In: Della Sala, Dominick A., Goldstein, Michael I. (Eds.), The Encyclopedia of the Anthropocene. vol. 2. Elsevier, Oxford, pp. 419–428.

Belle, J.H., Liu, Y., 2016. Evaluation of aqua MODIS Collection 6 AOD parameters for air quality research over the continental United States. Remote Sens. 8 (10), 815.

Bilal, M., Nichol, J.E., 2015. Evaluation of MODIS aerosol retrieval algorithms over the Beijing-Tianjin-Hebei region during low to very high pollution events. J. Geophys. Res.-Atmos. 120 (15), 7941–7957.

Burney, J., Ramanathan, V., 2014. Recent climate and air pollution impacts on Indian agriculture. Proc. Natl. Acad. Sci. 111 (46), 16319–16324.

Cai, H., Feng, X., Chen, Q., Sun, Y., Wu, Z., Tie, X., 2017. Spatial and temporal features of the frequency of cloud occurrence over China based on CALIOP. Adv. Meteorol. 2017.

Di, Q., Kloog, I., Koutrakis, P., Lyapustin, A., Wang, Y., Schwartz, J., 2016. Assessing PM2.5 exposures with high spatiotemporal resolution across the continental United States. Environ. Sci. Technol. 50 (9), 4712–4721.

Dubovik, O., King, M.D., 2000. A flexible inversion algorithm for retrieval of aerosol optical properties from Sun and sky radiance measurements. J. Geophys. Res.-Atmos. 105 (D16), 20673–20696.

Evans, J., van Donkelaar, A., Martin, R.V., Burnett, R., Rainham, D.G., Birkett, N.J., Krewski, D., 2013. Estimates of global mortality attributable to particulate air pollution using satellite imagery. Environ. Res. 120, 33–42.

Gautam, R., Hsu, N.C., Lau, K.M., 2010. Premonsoon aerosol characterization and radiative effects over the Indo-Gangetic Plains: implications for regional climate warming. J. Geophys. Res.-Atmos. 115 (D17).

Gupta, P., Remer, L.A., Levy, R.C., Mattoo, S., 2018. Validation of MODIS 3 km land aerosol optical depth from NASA's EOS Terra and Aqua missions. Atmos. Meas. Tech. 11 (5), 3145.

Han, S., Bian, H., Zhang, Y., Wu, J., Wang, Y., Tie, X., Li, Y., Li, X., Yao, Q., 2012. Effect of aerosols on visibility and radiation in spring 2009 in Tianjin, China. Aerosol Air Qual. Res. 12, 211–217.

Hansen, J., Sato, M., Ruedy, R., 1997. Radiative forcing and climate response. J. Geophys. Res.-Atmos. 102 (D6), 6831–6864.

Hoff, R.M., Christopher, S.A., 2009. Remote sensing of particulate pollution from space: have we reached the promised land? J. Air Waste Manage. Assoc. 59 (6), 645–675.

Holben, B.N., Eck, T.F., Slutsker, I., Tanre, D., Buis, J.P., Setzer, A., Vermote, E., Reagan, J.A., Kaufman, Y.J., Nakajima, T., Lavenu, F., 1998. AERONET—a federated instrument network and data archive for aerosol characterization. Remote Sens. Environ. 66 (1), 1–16.

Hsu, N.C., Tsay, S.C., King, M.D., Herman, J.R., 2004. Aerosol properties over bright-reflecting source regions. IEEE Trans. Geosci. Remote Sens. 42 (3), 557–569.

Hsu, N.C., Jeong, M.J., Bettenhausen, C., Sayer, A.M., Hansell, R., Seftor, C.S., Huang, J., Tsay, S.C., 2013. Enhanced Deep Blue aerosol retrieval algorithm: the second generation. J. Geophys. Res.-Atmos. 118 (16), 9296–9315.

Just, A.C., Wright, R.O., Schwartz, J., Coull, B.A., Baccarelli, A.A., Tellez-Rojo, M.M., Moody, E., Wang, Y., Lyapustin, A., Kloog, I., 2015. Using high-resolution satellite aerosol optical depth to estimate daily PM2.5 geographical distribution in Mexico City. Environ. Sci. Technol. 49 (14), 8576–8584.

Kahn, R.A., Gaitley, B.J., 2015. An analysis of global aerosol type as retrieved by MISR. J. Geophys. Res.-Atmos. 120 (9), 4248–4281.

Kaufman, Y.J., Tanré, D., Boucher, O., 2002. A satellite view of aerosols in the climate system. Nature 419 (6903), 215.

King, M.D., Platnick, S., Menzel, W.P., Ackerman, S.A., Hubanks, P.A., 2013. Spatial and temporal distribution of clouds observed by MODIS onboard the Terra and Aqua satellites. IEEE Trans. Geosci. Remote Sens. 51 (7), 3826–3852.

Kloog, I., Chudnovsky, A.A., Just, A.C., Nordio, F., Koutrakis, P., Coull, B.A., Lyapustin, A., Wang, Y., Schwartz, J., 2014. A new hybrid spatio-temporal model for estimating daily multi-year PM2.5 concentrations across northeastern USA using high resolution aerosol optical depth data. Atmos. Environ. 95, 581–590.

Kloog, I., Sorek-Hamer, M., Lyapustin, A., Coull, B., Wang, Y., Just, A.C., Schwartz, J., Broday, D.M., 2015. Estimating daily PM2.5 and PM10 across the complex geo-climate region of Israel using MAIAC satellite-based AOD data. Atmos. Environ. 122, 409–416.

Kumar, M., Singh, R.S., Banerjee, T., 2015a. Associating airborne particulates and human health: exploring possibilities: comment on: Kim, Ki-Hyun, Kabir, E. and Kabir, S. 2015. A review on the human health impact of airborne particulate matter. Environment International 74 (2015) 136–143. Environ. Int. 84, 201.

Kumar, M., Tiwari, S., Murari, V., Singh, A.K., Banerjee, T., 2015b. Wintertime characteristics of aerosols at middle Indo-Gangetic Plain: impacts of regional meteorology and long range transport. Atmos. Environ. 104, 162–175.

Kumar, M., Raju, M.P., Singh, R.S., Banerjee, T., 2017. Impact of drought and normal monsoon scenarios on aerosol induced radiative forcing and atmospheric heating in Varanasi over middle Indo-Gangetic Plain. J. Aerosol Sci. 113, 95–107.

Kumar, M., Parmar, K.S., Kumar, D.B., Mhawish, A., Broday, D.M., Mall, R.K., Banerjee, T., 2018. Long-term aerosol climatology over Indo-Gangetic Plain: trend, prediction and potential source fields. Atmos. Environ. 180, 37–50. https://doi.org/10.1016/j.atmosenv.2018.02.027.

Lau, K.M., Kim, K.M., 2006. Observational relationships between aerosol and Asian monsoon rainfall, and circulation. Geophys. Res. Lett. 33 (21).

Lee, H.J., Chatfield, R.B., Strawa, A.W., 2016. Enhancing the applicability of satellite remote sensing for PM2.5 estimation using MODIS deep blue AOD and land use regression in California, United States. Environ. Sci. Technol. 50 (12), 6546–6555.

Levy, R.C., Remer, L.A., Mattoo, S., Vermote, E.F., Kaufman, Y.J., 2007. Second-generation operational algorithm: retrieval of aerosol properties over land from inversion of Moderate Resolution Imaging Spectroradiometer spectral reflectance. J. Geophys. Res.-Atmos. 112 (D13).

Levy, R.C., Remer, L.A., Kleidman, R.G., Mattoo, S., Ichoku, C., Kahn, R., Eck, T.F., 2010. Global evaluation of the Collection 5 MODIS dark-target aerosol products over land. Atmos. Chem. Phys. 10 (21), 10399–10420.

Levy, R.C., Mattoo, S., Munchak, L.A., Remer, L.A., Sayer, A.M., Patadia, F., Hsu, N.C., 2013. The Collection 6 MODIS aerosol products over land and ocean. Atmos. Meas. Tech. 6 (11), 2989.

Levy, R.C., Mattoo, S., Sawyer, V., Shi, Y., Colarco, P.R., Lyapustin, A.I., Wang, Y., Remer, L.A., 2018. Exploring systematic offsets between aerosol products from the two MODIS sensors. Atmos. Meas. Tech. 11 (7), 4073–4092.

Liang, F., Xiao, Q., Wang, Y., Lyapustin, A., Li, G., Gu, D., Pan, X., Liu, Y., 2018. MAIAC-based long-term spatiotemporal trends of PM2.5 in Beijing, China. Sci. Total Environ. 616, 1589–1598.

Lyapustin, A., Martonchik, J., Wang, Y., Laszlo, I., Korkin, S., 2011a. Multiangle implementation of atmospheric correction (MAIAC): 1. Radiative transfer basis and look-up tables. J. Geophys. Res.-Atmos. 116 (D3).

Lyapustin, A., Wang, Y., Laszlo, I., Kahn, R., Korkin, S., Remer, L., Levy, R., Reid, J.S., 2011b. Multiangle implementation of atmospheric correction (MAIAC): 2. Aerosol algorithm. J. Geophys. Res.-Atmos. 116 (D3).

Lyapustin, A., Korkin, S., Wang, Y., Quayle, B., Laszlo, I., 2012. Discrimination of biomass burning smoke and clouds in MAIAC algorithm. Atmos. Chem. Phys. 12 (20), 9679–9686.

Lyapustin, A.I., Wang, Y., Laszlo, I., Hilker, T., Hall, F.G., Sellers, P.J., Tucker, C.J., Korkin, S.V., 2012. Multi-angle implementation of atmospheric correction for MODIS (MAIAC): 3. Atmospheric correction. Remote Sens. Environ. 127, 385–393.

Lyapustin, A., Alexander, M.J., Ott, L., Molod, A., Holben, B., Susskind, J., Wang, Y., 2014. Observation of mountain lee waves with MODIS NIR column water vapor. Geophys. Res. Lett. 41 (2), 710–716.

Lyapustin, A., Wang, Y., Korkin, S., Huang, D., 2018. MODIS Collection 6 MAIAC algorithm. Atmos. Meas. Tech. 11, 5741–5765. https://doi.org/10.5194/-11-5741-2018. (Discussion).

Martin, R.V., 2008. Satellite remote sensing of surface air quality. Atmos. Environ. 42 (34), 7823–7843.

Martins, V.S., Lyapustin, A., de Carvalho, L.A.S., Barbosa, C.C.F., Novo, E.M.L.M., 2017. Validation of high-resolution MAIAC aerosol product over South America. J. Geophys. Res. Atmos. 122. https://doi.org/10.1002/2016JD026301.

Mhawish, A., Banerjee, T., Broday, D.M., Misra, A., Tripathi, S.N., 2017. Evaluation of MODIS Collection 6 aerosol retrieval algorithms over Indo-Gangetic Plain: implications of aerosols types and mass loading. Remote Sens. Environ. 201, 297–313.

Mhawish, A., Kumar, M., Mishra, A.K., Srivastava, P.K., Banerjee, T., 2018. Remote sensing of aerosols from space: retrieval of properties and applications. In: Remote Sensing of Aerosols, Clouds, and Precipitation, pp. 45–83.

Munchak, L.A., Levy, R.C., Mattoo, S., Remer, L.A., Holben, B.N., Schafer, J.S., Hostetler, C.A., Ferrare, R.A., 2013. MODIS 3 km Aerosol Product: Applications Over Land in an Urban/Suburban Region.

Nichol, J.E., Bilal, M., 2016. Validation of MODIS 3 km resolution aerosol optical depth retrievals over Asia. Remote Sens. 8 (4), 328.

O'Neill, N.T., Eck, T.F., Holben, B.N., Smirnov, A., Dubovik, O., Royer, A., 2001. Bimodal size distribution influences on the variation of Angstrom derivatives in spectral and optical depth space. J. Geophys. Res.-Atmos. 106 (D9), 9787–9806.

Ramanathan, V., Ramana, M.V., 2005. Persistent, widespread, and strongly absorbing haze over the Himalayan foothills and the Indo-Gangetic Plains. Pure Appl. Geophys. 162 (8–9), 1609–1626.

Ramanathan, V.C.P.J., Crutzen, P.J., Kiehl, J.T., Rosenfeld, D., 2001. Aerosols, climate, and the hydrological cycle. Science 294 (5549), 2119–2124.

Reid, J.S., Eck, T.F., Christopher, S.A., Koppmann, R., Dubovik, O., Eleuterio, D.P., Holben, B.N., Reid, E.A., Zhang, J., 2005. A review of biomass burning emissions part III: intensive optical properties of biomass burning particles. Atmos. Chem. Phys. 5

(3), 827–849.
Remer, L.A., Kaufman, Y.J., Tanré, D., Mattoo, S., Chu, D.A., Martins, J.V., Li, R.R., Ichoku, C., Levy, R.C., Kleidman, R.G., Eck, T.F., 2005. The MODIS aerosol algorithm, products, and validation. J. Atmos. Sci. 62 (4), 947–973.
Remer, L.A., Mattoo, S., Levy, R.C., Munchak, L.A., 2013. MODIS 3 km aerosol product: algorithm and global perspective. Atmos. Meas. Tech. 6 (7), 1829.
Roujean, J.L., Leroy, M., Deschamps, P.Y., 1992. A bidirectional reflectance model of the Earth's surface for the correction of remote sensing data. J. Geophys. Res.-Atmos. 97 (D18), 20455–20468.
Russell, P.B., Kacenelenbogen, M., Livingston, J.M., Hasekamp, O.P., Burton, S.P., Schuster, G.L., Johnson, M.S., Knobelspiesse, K.D., Redemann, J., Ramachandran, S., Holben, B., 2014. A multiparameter aerosol classification method and its application to retrievals from spaceborne polarimetry. J. Geophys. Res.-Atmos. 119 (16), 9838–9863.
Sayer, A.M., Munchak, L.A., Hsu, N.C., Levy, R.C., Bettenhausen, C., Jeong, M.J., 2014. MODIS Collection 6 aerosol products: comparison between Aqua's e-Deep Blue, Dark Target, and "merged" data sets, and usage recommendations. J. Geophys. Res.-Atmos. 119 (24).
Sayer, A.M., Hsu, N.C., Bettenhausen, C., Jeong, M.J., Meister, G., 2015. Effect of MODIS Terra radiometric calibration improvements on Collection 6 Deep Blue aerosol products: validation and Terra/Aqua consistency. J. Geophys. Res.-Atmos. 120 (23).
Seinfeld, J.H., Bretherton, C., Carslaw, K.S., Coe, H., DeMott, P.J., Dunlea, E.J., Feingold, G., Ghan, S., Guenther, A.B., Kahn, R., Kraucunas, I., 2016. Improving our fundamental understanding of the role of aerosol–cloud interactions in the climate system. Proc. Natl. Acad. Sci. 113 (21), 5781–5790.
Sen, A., Abdelmaksoud, A.S., Ahammed, Y.N., Banerjee, T., Bhat, M.A., Chatterjee, A., Choudhuri, A.K., Das, T., Dhir, A., Dhyani, P.P., Gadi, R., 2017. Variations in particulate matter over Indo-Gangetic Plains and Indo-Himalayan Range during four field campaigns in winter monsoon and summer monsoon: role of pollution pathways. Atmos. Environ. 154, 200–224.
Singh, N., Murari, V., Kumar, M., Barman, S.C., Banerjee, T., 2017a. Fine particulates over South Asia: review and meta-analysis of PM2.5 source apportionment through receptor model. Environ. Pollut. 223, 121–136.
Singh, N., Mhawish, A., Deboudt, K., Singh, R.S., Banerjee, T., 2017b. Organic aerosols over Indo-Gangetic Plain: sources, distributions and climatic implications. Atmos. Environ. 157, 59–74.
Singh, N., Banerjee, T., Raju, M.P., Deboudt, K., Sorek-Hamer, M., Singh, R.S., Mall, R.K., 2018. Aerosol chemistry, transport and climatic implications during extreme biomass burning emissions over Indo-Gangetic Plain. Atmos. Chem. Phys. 18, 14197–14215.
Stafoggia, M., Schneider, A., Cyrys, J., Samoli, E., Andersen, Z.J., Bedada, G.B., Bellander, T., Cattani, G., Eleftheriadis, K., Faustini, A., Hoffmann, B., 2017. Association between short-term exposure to ultrafine particles and mortality in eight European urban areas. Epidemiology 28 (2), 172–180.
Superczynski, S.D., Kondragunta, S., Lyapustin, A.I., 2017. Evaluation of the multi-angle implementation of atmospheric correction (MAIAC) aerosol algorithm through intercomparison with VIIRS aerosol products and AERONET. J. Geophys. Res.-Atmos. 122 (5), 3005–3022.
Tanré, D., Kaufman, Y.J., Herman, M., Mattoo, S., 1997. Remote sensing of aerosol properties over oceans using the MODIS/EOS spectral radiances. J. Geophys. Res.-Atmos. 102 (D14), 16971–16988.
Tao, M., Chen, L., Wang, Z., Wang, J., Che, H., Xu, X., Wang, W., Tao, J., Zhu, H., Hou, C., 2017. Evaluation of MODIS Deep Blue aerosol algorithm in desert region of East Asia: ground validation and intercomparison. J. Geophys. Res.-Atmos. 122 (19).
Tian, R., An, J., 2013. Relationship between aerosol transport routes and red tide occurrences in the East China Sea. Environ. Earth Sci. 69 (5), 1499–1508.
Torres, O., Tanskanen, A., Veihelmann, B., Ahn, C., Braak, R., Bhartia, P.K., Veefkind, P., Levelt, P., 2007. Aerosols and surface UV products from Ozone Monitoring Instrument observations: an overview. J. Geophys. Res.-Atmos. 112 (D24).
Wang, J., Martin, S.T., 2007. Satellite characterization of urban aerosols: importance of including hygroscopicity and mixing state in the retrieval algorithms. J. Geophys. Res.-Atmos. 112 (D17).
Winker, D.M., Pelon, J., Coakley Jr., J.A., Ackerman, S.A., Charlson, R.J., Colarco, P.R., Flamant, P., Fu, Q., Hoff, R.M., Kittaka, C., Kubar, T.L., 2010. The CALIPSO mission: a global 3D view of aerosols and clouds. Bull. Am. Meteorol. Soc. 91 (9), 1211–1230.
Xiao, Q., Wang, Y., Chang, H.H., Meng, X., Geng, G., Lyapustin, A., Liu, Y., 2017. Full-coverage high-resolution daily PM2.5 estimation using MAIAC AOD in the Yangtze River Delta of China. Remote Sens. Environ. 199, 437–446.